Hu *et al. Cancer & Metabolism* (2025) 13:32
https://doi.org/10.1186/s40170-025-00401-6

Cancer & Metabolism

RESEARCH Open Access

NRF2 maintains redox balance via ME1 and NRF2 inhibitor synergizes with venetoclax in NPM1-mutated acute myeloid leukemia

Jiayuan Hu[1†], Zihao Yuan[1†], Yan Shu[2†], Jun Ren[1], Jing Yang[1], Lisha Tang[1], Xingyu Wei[1], Yongcan Liu[1], Fangfang Jin[1], Qiaoling Xiao[1], Xinyi Chen[1], Nan Wu[1], Wen Zhao[1], Ziwei Li[2*] and Ling Zhang[1*]

Abstract

Background Acute myeloid leukemia (AML) with nucleophosmin 1 (*NPM1*) mutations represents a distinct subtype of leukemia. Emerging evidence suggests that regulation of redox metabolism contributes to tumorigenesis and reveals a metabolic vulnerability in anti-tumor therapies. However, the role of redox homeostasis between reactive oxygen species (ROS) and antioxidant systems plays in NPM1-mutated AML has not been fully elucidated.

Methods First, ROS-related metabolic pathways in NPM1-mutated AML were analyzed using RNA-sequencing data. Intracellular and mitochondrial ROS levels in leukemia cells were detected using flow cytometry (FCM). The expression of nuclear factor (erythroid-derived 2)-like 2 (NRF2) was analyzed in public databases and further validated in AML primary blasts and cell lines by quantitative real-time PCR (qRT-PCR), western blotting, and immunofluorescence. Next, the mechanism underlying NRF2 expression was investigated through the RNA immunoprecipitation (RIP), methylated RNA immunoprecipitation (MeRIP) and rescue experiments. Additionally, the downstream target gene of NRF2 was identified by bioinformatics analysis and chromatin immunoprecipitation (ChIP) assays. Furthermore, RNA interference and the NRF2 inhibitor ML385 were applied to explore the role of NRF2 in leukemia. Finally, the anti-leukemic effects of ML385 alone or in combination with the B-cell lymphoma 2 (BCL-2) inhibitor venetoclax on AML cells were investigated using FCM analysis and western blotting, and further explored in cell line-derived xenograft (CDX) mouse models.

Results In this study, we identified significant ROS accumulation in leukemia cells with *NPM1* mutations. Meanwhile, elevated NRF2 expression and its nuclear localization were observed in NPM1-mutated AML cells. The high NRF2 expression levels were at least partially induced by fat mass and obesity-associated protein (FTO) via m^6A modification. Functionally, NRF2 exerts its antioxidant effects by transcriptionally upregulating malic enzyme 1 (ME1) expression and enhancing its activity. Targeting NRF2/ME1 axis reduced NADPH/$NADP^+$ ratio, increased ROS levels,

†Jiayuan Hu, Zihao Yuan and Yan Shu contributed equally to this work.

*Correspondence:
Ziwei Li
liziwei1989@cqu.edu.cn
Ling Zhang
lingzhang@cqmu.edu.cn

Full list of author information is available at the end of the article

impaired leukemia cell viability, and promoted apoptosis. More importantly, NRF2 inhibitor ML385 in combination with venetoclax showed synergistic anti-leukemic activity in vitro and in vivo.

Conclusion Overall, our findings provide new insight into the therapeutic potential of targeting NRF2 and guide the development of innovative combination therapies in NPM1-mutated AML.

Keywords Acute myeloid leukemia, Nucleophosmin 1, NRF2, ME1, Redox homeostasis, Venetoclax

Background

Acute myeloid leukemia (AML) is a hematological malignancy characterized by the uncontrolled proliferation of myeloid cells in the blood, bone marrow, and other tissues [1, 2]. The nucleolar chaperone nucleophosmin 1 (NPM1) mutations are detected in approximately 50% of AML patients with normal karyotypes [3, 4]. In recent years, significant progress has been made in the development of targeted therapies against NPM1-mutated AML [5]. However, elderly patients with NPM1-mutated AML treated with intensive chemotherapy exhibit only 15–20% long-term survival [6, 7]. Therefore, it is essential to explore the underlying molecular mechanisms and search for novel therapeutic strategies for this particular AML subgroup.

Tumor cells typically exhibit aberrant redox metabolism with high reactive oxygen species (ROS) levels [8]. To survive under such oxidized conditions, cancer cells adapt by enhancing their antioxidant capacity to optimize ROS-driven proliferation and avoid ROS thresholds that trigger cell death [9]. Recently, several studies have demonstrated that certain types of cancer cells display an elevated oxidative status and may develop more dependency on antioxidant pathways [10–13]. A recent investigation also reported that stress pathways, including oxidative stress response, are activated in leukemia cells with *NPM1* mutations [14]. However, the role of ROS versus antioxidants in maintaining redox homeostasis, and whether reprogrammed ROS homeostasis establishes a targetable vulnerability in NPM1-mutated AML, remains unknown.

Recently, several researches have revealed the stratified response of the antioxidant transcription factor network to oxidative stress [15, 16]. Nuclear factor (erythroid-derived 2)-like 2 (NRF2, also called NFE2L2), a crucial antioxidant transcription factor, provides an initial adaptive response against oxidative stress by regulating a wide of antioxidant and detoxification genes [17]. Upon exposure to ROS, NRF2 translocates to the nucleus, where it binds to antioxidant response elements (AREs) by heterodimerizing with small musculoaponeurotic fibrosarcoma (sMAF) proteins, thereby activating the transcription of its target genes [18]. In parallel, NRF2 can be regulated either transcriptionally by oncogenes that alter its mRNA levels [19] or post-translationally by repressors that control its protein stability [20]. It has been proposed that the antioxidant transcriptional programs regulated by NRF2 include genes involved in NADPH production, GSH and thioredoxin systems, and quinone reduction [21]. Collectively, these programs help protect cancer cells from oxidative stress [21, 22] and chemotherapeutic agents [23]. Among these systems controlled by NRF2, NADPH-based redox couples are regarded as the center of antioxidant defences [16]. Malic enzyme 1 (ME1), a critical NADPH synthesis enzyme, generates cytosolic NADPH by catalyzing the oxidative decarboxylation of malate to pyruvate and CO_2 [24]. Therefore, a deeper investigation into the regulatory and functional roles of NRF2 in leukemia is imperative.

ML385 is a selective and innovative NRF2 inhibitor [25]. It has been shown to specifically bind the Neh1 domain of NRF2 that mediates NRF2 interaction with ARE regions, thereby inhibiting transcription of NRF2-dependent genes [26]. To date, several landmark studies have revealed that ML385 has significant anti-tumor activity in solid tumors [25, 27]. Recently, it has been reported that inducing cytotoxic oxidative stress, achieved through downregulation of antioxidant molecules, can sensitize leukemia cells to chemotherapeutic agents [28]. Venetoclax (VEN), a selective B-cell lymphoma 2 (BCL2) inhibitor, has been widely incorporated in the treatment of AML patients. Notably, recent researches have uncovered that NPM1-mutated AML benefits from venetoclax-based regimens [29, 30], but unfit patients relapsing after treatment represent a clinical challenge [5]. Of particular interest, our previous work demonstrated that venetoclax-based combination therapy may be a promising therapeutic option for AML [31, 32]. In light of these findings, we sought to investigate whether ML385 alone or in combination with VEN could exert the anti-leukemia effect in AML.

In this study, we first determined the elevated ROS burden and high expression of antioxidant regulator NRF2 in NPM1-mutated leukemia cells. Increased NRF2 expression was found to be partially driven by fat mass and obesity-associated protein (FTO)-mediated m^6A RNA demethylation. Furthermore, NRF2 activation led to the overexpression of ME1, thereby maintaining cellular redox homeostasis and promoting cell survival. Importantly, NRF2 inhibitor ML385 either alone or in combination with venetoclax showed anti-leukemic effects in

NPM1-mutated AML cells, supporting its potential as a potentially individualized therapeutic strategy.

Materials and methods

Cell culture and treatment

The OCI-AML2 and OCI-AML3 (carrying NPM1 mutation type A [NPM1-mA]), both human myeloid leukemia cells, were bought from Deutsche Sammlung von Mikroorganismen und Zellkulturen GmbH (DSMZ, Braun schweig, NI, Germany). Cells were cultivated in RPMI-160 medium (Thermo Fisher Scientific, Waltham, MA, USA, #11875093) supplemented with 10% fetal bovine serum (FBS) (Thermo FishFisher Scientific, #10099141 C) and 1% penicillin-streptomycin solution (P-S) (Beyotime, Shanghai, China, #C0222). THP-1 and HL-60, human myeloid leukemia cells, were purchased from American Type Culture Collection (ATCC, Manassas, VA, USA) and cultured in RPMI-1640 medium containing 10% FBS and 1% P-S.

Cells were treated with the following compounds as indicated: the proteasome inhibitor MG-132 (Topscience, Shanghai, China, #T2154); two FTO demethylase activity inhibitors, meclofenamic acid (MA) (Selleck, Houston, TX, USA, #S4295) and FB23-2 (Selleck, #S8837); the NRF2 inhibitor ML385 (MCE, Monmouth Junction, NJ, USA, #HY-100523); the BCL2 inhibitor venetoclax (MCE, Monmouth Junction, NJ, USA, #HY-15531) and then collected for analysis.

Establishment of stable cell lines

For overexpression analysis, the lentiviral vectors expressing wild-type NPM1 (NPM1-wt) and NPM1-mA sequence were obtained from Genechem (Shanghai, China). To achieve ectopic expression of FTO, a lentivirus overexpressing FTO (OE-FTO) and empty control vectors (OE-NC) were purchased from Genechem (Shanghai, China). Short hairpin RNA (shRNA) construct targeting NPM1 and FTO were acquired from Genechem (Shanghai, China), while shRNA constructs targeting NRF2 were obtained from GenePharma (Shanghai, China). All lentivirus vectors express GFP and carry purinomycin-resistance genes to monitor the transfection efficiency. Leukemia cells were seeded into a 24-well plate and transfected with lentivirus in the presence of HitransG P transduction enhancer (Genechem, #REVG005) for 72 h. The puromycin-resistant cells were selected by culturing in puromycin-containing medium for 7 days and subsequently expanded for further analyses. For knockdown analysis, the lentivirus-mediated shRNA sequences used are listed in the Table 1.

Table 1 The lentivirus-mediated short hairpin RNA (shRNA) sequences for each gene used in this study

Genes	Sequences(5′-3′)
NPM1	shNPM1#1: 5′-GCCGACAAAGATTATCACTTT-3′ shNPM1#2: 5′-AGCAAGGTTCCACAGAAAA-3′
FTO	shFTO#1: 5′-GACAAAGCCTAACCTACTT-3′ shFTO#2: 5′-GAGCTTTGAGTCCTATGCT-3′
NRF2	shNRF2#1: 5′-CATACTTTGGAGGCAAGATAT-3′ shNRF2#2: 5′-GATGAAGAGACAGGTGAATTT-3′

RNA isolation and quantitative real-time polymerase chain reaction (qRT-PCR)

Total RNA was extracted using TRIzol reagent (Takara, Kyoto, Japan) and reverse transcribed into cDNA using PrimeScript™ RT Master Mix (Takara, #RR036A) according to the manufacturer's protocol. qRT-PCR was performed using SYBR Green™ Premix Ex Taq™ II (Tli RNaseH Plus) (Takara, #RR820A) on the CFX Connect™ Real-Time PCR Detection System (Bio-Rad). Cycling conditions were as follows: 30 s at 95 ℃ for the initial denaturation, and amplification was operated with 39 cycles of 5 s at 95 ℃, 30 s at 58 ℃, 20 s at 72 ℃, and finally 10 min at 72 ℃ for the extension. The mRNA expression levels were calculated using the $2^{-\Delta\Delta Ct}$ method and β-actin was used as a normalized standard control. The primers for *ME1-AREs* used in the ChIP experiments were adopted from Lee D et al. [33]. Primer sequences are listed in Table 2.

Western blotting

The treated cells were collected and lysed in the RIPA lysis buffer (Beyotime, Shanghai, China, #P0013C) with protease inhibitor (Bimake, Houston, TX, USA, #B14001). The total protein was kept on ice for 30 min and then clarified through centrifugation at 13,300 rpm for 30 min at 4 ℃. Nuclear and cytosolic protein fractions were extracted using the Nuclear and Cytoplasmic Protein Extraction Kit (Beyotime, Shanghai, China, #P0027) according to the manufacturer's instructions. Briefly, the protein concentrations were measured using the BCA Protein Assay Kit (Beyotime, Shanghai, China, #P0010S), and samples were boiled in 5× sodium dodecyl sulfate-polyacrylamide gelelectrophoresis (SDS-PAGE) loading buffer (Beyotime, Shanghai, China, #P0015). The proteins were separated on 12% SDS-PAGE and transferred onto polyvinylidene fluoride (PVDF) membranes (Bio-Rad, #1620177). Then the membranes were blocked with 5% non-fat milk at room temperature for 2 h and incubated with the indicated primary antibodies at 4 ℃ overnight. After being washed with tris-buffered saline containing 0.02% Tween-20 (TBST) for three times, the membranes were incubated with horseradish peroxidase (HRP)-conjugated goat anti-rabbit IgG (Biosharp, Beijing, China, #BL003A) or HRP-conjugated goat anti-mouse IgG (Biosharp, Beijing, China, #BL001A) at 1:4000 dilution at room temperature for 1 h. The protein bands were detected using an enhanced chemiluminescence (ECL)

Table 2 The PCR primer sequences for each gene used in this study

Genes	Sequences(5′-3′)
NPM1-wt	F: 5′-ACGGTCAGTTTAGGGGCTG-3′ R: 5′-CTGTGGAACCTTGCTACCACC-3′
NPM1-mA	F: 5′-TGGAGGTGGTAGCAAGGTTC-3′ R: 5′-CTTCCTCCACTGCCAGACAGA-3′
NRF2	F: 5′-TCAGCGACGGAAAGAGTATGA-3′ R: 5′-CCACTGGTTTCTGACTGGATGT-3′
FTO	F:5′-ACTTGGCTCCCTTATCTGACC-3′ R: 5′-TGTGCAGTGTGAGAAAGGCTT-3′
ME1	F: 5′-CTGCTGACACGGAACCCTC-3′ R:5′-GATCTCCTGACTGTTGAAGGAAG-3′
HO1	F:5′-AAGACTGCGTTCCTGCTCAAC-3′ R:5′-AAAGCCCTACAGCAACTGTCG-3
NQO1	F:5′-GAAGAGCACTGATCGTACTGGC-3′ R:5′-GGATACTGAAAGTTCGCAGGG-3′
GCLC	F:5′-ATGGAGGTGCAATTAACAGAC-3′ R: 5′-ACTGCATTGCCACCTTTGCA-3′
GCLM	F:5′-TGTCTTGGAATGCACTGTATCTC-3′ R:5′-CCCAGTAAGGCTGTAAATGCTC-3′
β-actin	F: 5′-TAGTTGCGTTACACCCTTTCTTG-3′ R: 5′-TGCTGTCACCTTCACCGTTC-3′
ME1-ARE 1 (ChIP)	F: 5′-CTGATGGCATTCTCACCTGTG-3′ R: 5′-TGCCTTGTAACAAACTGTGGT-3′
ME1-ARE 2 (ChIP)	F: 5′-CAGGCGAGGTCAAAGAAGC-3′ R: 5′-GCCCCAGTTTCCTTTTCAGTT-3′
ME1-ARE 3 (ChIP)	F: 5′-TGCCAGGACTCGCTCTTC-3′ R: 5′-CGAGAAGCGCTGAGTCATG-3′
ME1-ARE 4 (ChIP)	F: 5′-CAGTCAGCACCGTCACCC-3′ R: 5′-TTGTTGAGGTGAGGGTTCCG-3′

F stands for forward; R stands for reverse; *NPM1-mA* stands for NPM1 mutation type A; *NPM1-wt* stands for NPM1 wild-type; *ARE* stands for antioxidant response element

solution. β-actin was served as a loading control. The following antibodies were used in the study: anti-NRF2 (1:5000, #16396-1-AP), anti-ME1 (1:1000, #16619-1-AP), anti-FTO (1;1000, #27226-1-AP) were purchased from Proteintech (Wuhan, China); anti-NPM1-mA (1:1000, #PA1-46356), anti-NPM1 (1:1000, #MA3-25200-A488) were purchased from invitrogen; anti-Histon H3 (1:1000, #M1309-1) was purchased from HUABIO (Hangzhou, China); anti-BCL2 (1:1000, #A5010), anti-CASP3 (1:1000, #A5185) were purchased from Selleckchem; anti-BAX (1:1000, #A51310200020010) was purchased from Bimake; anti-Cleaved CASP3 (1:1000, #9664T) was purchased from Cell Signaling Technology (Danvers, MA, USA); anti-β-actin (1:1000, #TA-09) was purchased from ZSGB-BIO (Beijing, China); HRP-conjugated goat anti-rabbit IgG (1:4000, #BL003A) and HRP-conjugated goat anti-mouse IgG (1:4000, #BL001A) were purchased from Biosharp (Beijing, China).

RNA sequencing

OCI-AML2 cells overexpressing NPM1-mA and OCI-AML2 cells transfected with an empty vector were collected at a density of 1×10^6 cells. The total RNA of cells was prepared by TRIzol reagent (Thermo Fisher Scientific, #15596026). RNA sequencing was performed by BGI Genomics Co., Ltd (China) on the BGISEQ platform. Each group included three biological replicates.

Bioinformatics analysis

The gene expression of RNA sequencing was quantified using fragments per kilobase of exon model per million mapped reads (FPKM). Gene Set Enrichment Analysis (GSEA) was conducted and visualized by R package clusterProfiler, based on Gene Ontology (GO) gene sets. The bubble plot was plotted by an online visualization platform (https://www.bioinformatics.com.cn). Gene expression profiles and clinical characteristics of AML patients were retrieved from the NCBI Gene Expression Omnibus (GEO, https://www.ncbi.nlm.nih.gov/gds) database under the accession numbers GSE68466 ($n = 109$), The Cancer Genome Atlas (TCGA, $n = 86$, http://www.cancergenome.nih.gov) and Beat AML (http://vizome.org/additional_figures_BeatAML.html, $n = 100$) databases. The Kaplan-Meier survival analysis was performed using the Kaplan-Meier plotter (http://kmplot.com) to investigate the association between NRF2 expression and survival outcomes in NPM1-mutated AML. Additionally, NPM1-mutated AML patients from Beat AML database were divided into high and low gene expression groups based on the median expression levels of *ME1*, *HO1 (HMOX1)*, *NQO1*, *GCLC*, and *GCLM* levels at diagnosis as the cut-off criterion. Overall survival was defined as from the date of diagnosis to death in any cause. Correlations of mRNA expression between *FTO* and *NRF2 (NFE2L2)*, between *NRF2 (NFE2L2)* and *ME1* in AML patients using Gene Expression Profiling Interactive Analysis (GEPIA) were generated. Meanwhile, correlations of mRNA expression between *NRF2* (*NFE2L2*) and *ME1* in leukemia cell lines were assessed using the Cancer Cell Line Encyclopedia (CCLE) (https://sites.broadinstitute.org/ccle) database.

Measurement of ROS levels

Intracellular ROS and mitochondrial ROS levels were assessed using the fluorescent probes dihydroethidium (DHE) or Mitochondrial Superoxide Assay Kit with MitoSOX™ Red (MitoSOX). 1×10^6 leukemia were incubated with 5μM DHE (Beyotime, Shanghai, China, #S0063) or 5μM MitoSOX Red (Beyotime, Shanghai, China, #S0061S) at 37 ℃ for 30 min, respectively. ROS levels in cells was determined using a FACSCalibur™ flow cytometer (FCM, BD Biosciences, USA) and analyzed with Flowjo software.

Clinical samples

The bone marrow and peripheral blood samples from patients with newly diagnosed AML, as well as the healthy donor were obtained from the First Affiliated Hospital of Chongqing Medical University and Xinqiao Hospital of Third Military Medical University. The study was approved by the Ethics Committee of Chongqing Medical University and conducted in accordance with the the Declaration of Helsinki. The mononuclear cells were isolated by Ficoll mononuclear cell separation solution (Hao Yang Biological Manufacture Co., Tianjin, China, #TBD2013CHU05). Briefly, the samples were layered onto Ficoll solution and centrifuged at 450 × g for 30 min to form discrete layers. The mononuclear layer was collected and washed twice with phosphate-buffered saline (PBS). Total RNA from the mononuclear cells was isolated for further analysis. The clinical characteristics of AML patients were shown in Table 3.

Table 3 Clinical characteristics of primary AML patient samples

Patient	Gender	Age (year)	Disease Status	FAB subtype	Gene mutation
AML#1	Male	36	Newly diagnosed	M4	WT1/ABL
AML#2	Male	22	Newly diagnosed	M4	TP53, MLL, WT1
AML#3	Female	30	Newly diagnosed	M5	MLL-AF9
AML#4	Female	43	Newly diagnosed	M2	WT1/ABL
AML#5	Female	61	Newly diagnosed	M5	WT1/AL, MLL
AML#6	Male	59	Newly diagnosed	M4	WT1/ABL, MLL
AML#7	Male	53	Newly diagnosed	M5	WT1/AL
AML#8	Male	70	Newly diagnosed	M5	WT1/AL, TP53/CEP17
AML#9	Female	46	Newly diagnosed	M5	WT1/AL, NRAS
AML#10	Female	16	Newly diagnosed	M5	MLL-AF9, WT, MLL, TLT3-TKD
AML#11	Male	53	Newly diagnosed	M2a	SRSF2, CEBPA, ASXL1, PHF6, WT1
AML#12	Female	34	Newly diagnosed	M1	NPM1, WT1/ABL
AML#13	Male	28	Newly diagnosed	M1	NPM1, FLT3-ITD, IDH2
AML#14	Male	44	Newly diagnosed	M1	NPM1, WT1
AML#15	Male	69	Newly diagnosed	M5	NPM1, SRSF2, TET2, FLT3-ITD, SH2B3, JAK2, WT1
AML#16	Male	52	Newly diagnosed	M2	NPM1, WT1, IDH2, CEBPA

Immunofluorescence

The cells were collected onto slides and washed with cold PBS for three times, then fixed in 4% paraformaldehyde (Biosharp, Beijing, China, #BL539A) for 20 min at room temperature. This was followed by permeabilization with 0.1% Triton X-100 for 15 min. Fixed cells were blocked in 10% fetal sheep serum (BOSTER, Wuhan, China, #AR0009) for 30 min and then incubated with an anti-NRF2 antibody (Proteintech, Wuhan, China, #16396-1-AP) at 4 ℃ overnight. The next day, the cells were washed with PBS for three times and then incubated with Coralite 594-conjugated goat anti-rabbit secondary antibody (Proteintech, Wuhan, China, #SA00013-4) for 1 h at room temperature. Subsequently, 4',6-diamino-2-phenylindole (DAPI) (Beyotime, Shanghai, China, #1005) was used for the nucleus staining. The stained cells were observed utilizing a fluorescence microscope (Nikon, Tokyo, Japan).

RNA-binding protein immunoprecipitation (RIP) assays

The RIP assays were performed using the RNA Immunoprecipitation Kit (GENESEED, Guangzhou, China, #P0101) to investigate the interaction between *NRF2* mRNA and FTO. A total of 1×10^7 cells were lysed in RIP lysis buffer supplemented with protease and RNase inhibitors. Then the lysates were incubated with protein A/G beads conjugated to the anti-FTO rabbit polyclonal antibody (Proteintech, Wuhan, China, #27226-1-AP), anti-m^{6}A rabbit polyclonal antibody (Abcam, Cambridge, United Kingdom, #ab286164) or control IgG (Cell Signaling Technology, Danvers, MA, USA, #2729S) for 16 h at 4 ℃. The target RNA was eluted and was finally extracted for qRT-PCR analysis.

mRNA stability assays

To assess *NRF2* mRNA stability, cells were treated with 5 μg/mL actinomycin D (Act-D) (Adooq Bioscience, Irvine, USA, #A13239) for 0, 2, 4, 6, or 8 h. Then total RNA was extracted at each time point and subjected to qRT-PCR analysis.

Measurement of NADPH/NADP$^+$ ratio and ME1 activity

The intracellular NADPH/NADP$^+$ ratio was measured using the NADP$^+$/NADPH Assay Kit with WST-8 (Beyotime, Shanghai, China, #S0179). ME1 activity in AML cells was measured using the NADP Malic Enzyme (NADP-ME) Activity Assay Kit (Solarbio, Beijing, China, #BC1125) in accordance with the manufacturers' instructions.

Chromatin immunoprecipitation (ChIP) assays

ChIP assays were performed to verify the binding of NRF2 to the AREs within the ME1 promoter region using BeyoChIP™ Enzymatic ChIP Assay Kit (Beyotime,

Shanghai, China, #P2083S). In brief, 1×10^7 cells were collected from each group, and treated with 37% formaldehyde at room temperature for 10 min, followed by quenching with 125 mM glycine for 5 min. The cells were then harvested, and chromatin was enzymatically digested with micrococcal nuclease (MNase) to obtain 150–900 bp fragments. After cell lysis, immunoprecipitation was performed overnight at 4 °C with either an anti-NRF2 antibody (Proteintech, Wuhan, China, #16396-1-AP) or a negative control IgG antibody (Cell Signaling Technology, Danvers, MA, USA, #2729S). Subsequently, protein-DNA cross-links were reversed by incubation at 65 °C for 2 h, and proteins were digested with proteinase K. The immunoprecipitated DNA was purified and quantified by qRT-PCR using primers listed in Table 2.

Cell transfection

The short interfering RNA (siRNA) targeting ME1 (siME1) and control siRNA (siNC) were synthesized by GenePharma (Shanghai, China). For transfections, 2.5×10^5 cells per well were plated into a 24-well plate and transfected using Lipofectamine 2000™ Transfection Reagent (Invitrogen, Carlsbad, CA, USA, #11668500) according to the manufacturer's instructions. The siRNA targeting sequence for human ME1 were 5'-GGGCAT ATTGCTTCAGTTC-3' (designated as siME1#1) and 5'-GCCTTCAATGAACGGCCTATT-3' (designated as siME1#2).

Cell counting kit-8 (CCK-8) assays

Cell viability was assessed using the Cell Counting Kit-8 (CCK-8) Kit (Solarbio, Beijing, China, #CA1210). The lentivirus-infected cells or reagent-treated AML cells were plated in 96-well plates at a density of 1.5×10^4 cells/well. The cells cultured in RPMI-1640 medium containing 10% FBS. At the indicated time points, each well was added into 10 μL CCK8 solution, and then the cells were incubated for 2–3 h at 37 ℃ in the dark. The absorbance at 450 nm was then measured using the microplate reader (BioTeck, CA, USA).

Cell apoptosis assays

The cell apoptosis was evaluated by the Annexin V-APC/DAPI Apoptosis Kit (Elabscience, Wuhan, China, #E-CK-A258) or the Annexin V-FITC/PI Apoptosis Kit (Elabscience, Wuhan, China, #E-CK-A211). Briefly, 1×10^6 cells were collected and washed with PBS, then stained according to the manufacturer's instructions. The stained cells were analyzed by a FACSCalibur™ flow cytometer (FCM, BD Biosciences, USA) and CytExpert software.

Cell cycle assays

The cell cycle distribution was assessed by the Cell Cycle Assay Kit (Elabscience, Wuhan, China, #E-CK-A351). The treated AML cells were collected, washed with pre-cooled PBS, and fixed in ice-cold 70% ethanol at 4 ℃ for 12 h. The fixed cells were stained using the Cell Cycle Kit in accordance with the manufacturer's instructions. Data were acquired on a FACSCalibur™ flow cytometer (FCM, BD Biosciences, USA) and disposed with ModFit LT software.

Animal experiments

Seven-week-old female NOD/SCID mice were purchased from GemPharmatech (China). NOD/SCID mice were injected via the tail vein with 2×10^6 OCI-AML3 cells per mouse and randomly assigned to four groups: vehicle control, 30 mg/kg ML385, 50 mg/kg venetoclax, or 30 mg/kg ML385 combined with 50 mg/kg venetoclax. The drugs were dissolved in 10% DMSO, 5% Tween-80, 40% PEG300 and sterile water, and were administered intraperitoneally once every two days. After 4 weeks, FCM analysis was used to examine human $CD45^+$ cells in the bone marrow from mice. The weights of the livers and spleen were recorded. Then the livers and spleens were obtained to observe infiltration of leukemia cells through swelling size, and then sectioned into 4 μm-thick sections, which were stained with hematoxylin and eosin (H&E). Bone marrow cells were harvested from femurs for Wright's staining and western blotting. The survival curves of mice were analyzed by the Kaplan-Meier method. The blood samples were drawn for biochemical tests. The animal experiments were approved by the Animal Care Ethics Committee of Chongqing Medical University.

Statistical analysis

Data were obtained from three independent experiments and the results were expressed as the mean ± SD. Statistical analyses were performed with GraphPad Prism software (Version 8.0). Comparisons between two groups were analyzed using the unpaired Student's t-tests, while comparisons among multiple groups were performed using the one-way analysis of variance (ANOVA). The Kaplan-Meier survival data were analyzed using the long-rank test. P-value < 0.05 was considered statistically significant ($^*p < 0.05$, $^{**}p < 0.01$, $^{***}p < 0.001$). No significance was defined as ns.

Results

ROS metabolic pathways are enhanced in NPM1-mutated leukemia cells

To explore the redox homeostasis in NPM1-mutated leukemia cells (OCI-AML2 cells overexpressing NPM1-mA and OCI-AML3 cells naturally harboring NPM1-mA),

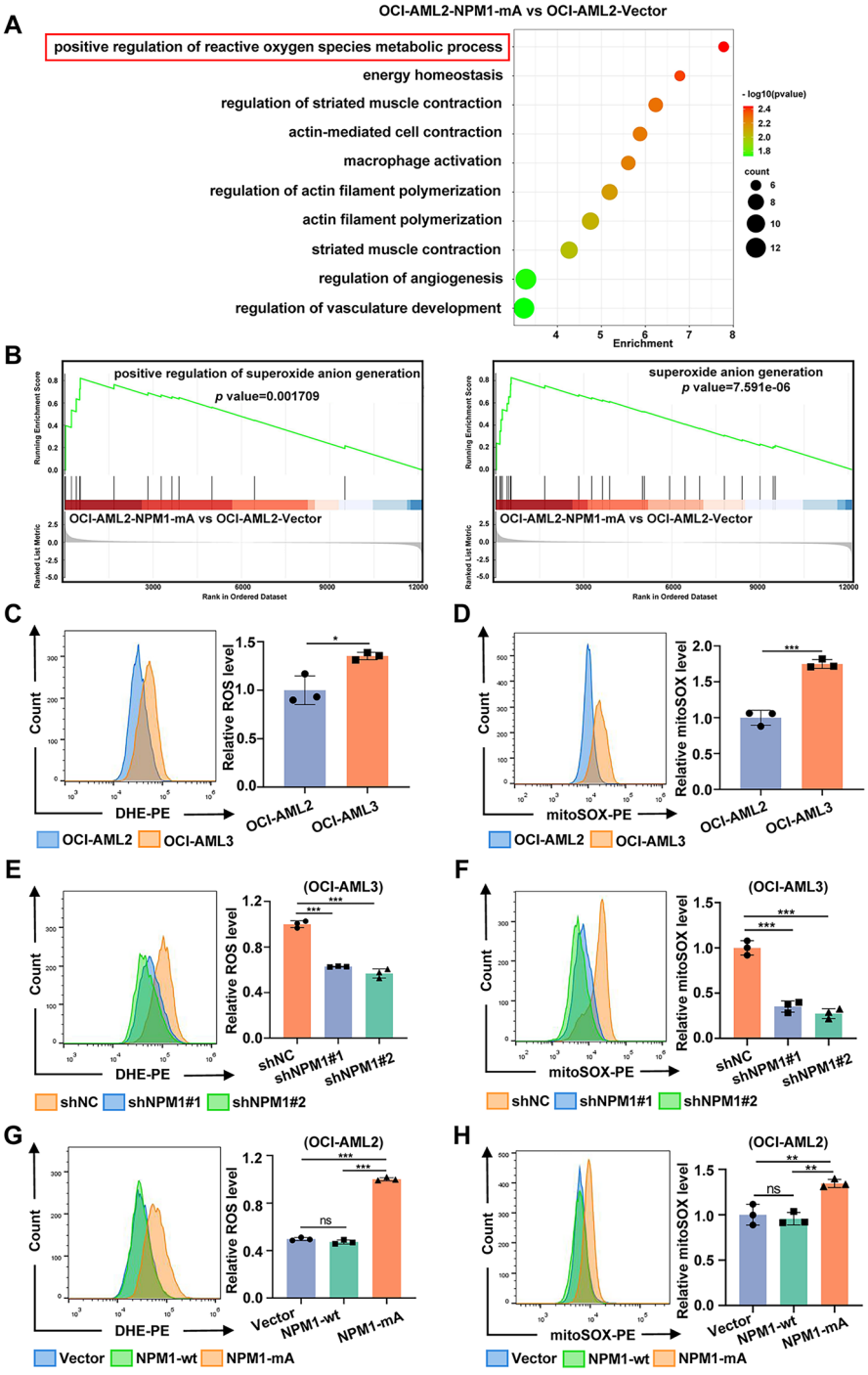

Fig. 1 ROS burden is increased in NPM1-mutated leukemia cells. **(A)** A scatter plot of the enriched up-regulated Gene Ontology (GO) pathways in OCI-AML2-NPM1-mA vs. OCI-AML2-vector is shown in the bubble plot, highlighting the pathways significantly enriched in NPM1-mA-overexpressing cells. **(B)** Gene set enrichment analysis (GSEA) showing differential enrichment of genes related to superoxide anion generation and positive regulation of superoxide anion generation. The data were from the RNA-seq. **(C)** Flow cytometry analysis of superoxide levels using DHE staining in leukemia cells. **(D)** Flow cytometry analysis of mitochondrial superoxide levels using MitoSOX Red staining in leukemia cells. **(E, G)** Flow cytometry analysis of superoxide levels using DHE staining in NPM1-mA-silenced OCI-AML3 cells **(E)** or in NPM1-wt-enforced OCI-AML2 and NPM1-mA-enforced OCI-AML2 cells **(G)**. **(F, H)** Flow cytometry analysis of mitochondrial superoxide levels using MitoSOX Red staining in NPM1-mA-silenced OCI-AML3 cells **(F)** or in NPM1-wt-enforced OCI-AML2 and NPM1-mA-enforced OCI-AML2 cells **(H)**. Data were presented as the mean ± SD of three independent experiments. *$p < 0.05$, **$p < 0.01$, ***$p < 0.001$, ns, not significant

we first performed Gene Ontology (GO) pathway analysis of RNA-sequencing data comparing OCI-AML2 cells with NPM1-mA overexpression and vector control. This analysis revealed the positive regulation of reactive oxygen species (ROS) metabolic process was significantly enriched in NPM1-mA-enforced OCI-AML2 cells (Fig. S1A and B, Fig. 1A). In addition, the gene set enrichment analysis (GSEA) showed significant enrichment of the positive regulation of superoxide anion (one kind of ROS) generation and the superoxide anion generation pathway in NPM1-mA-overexpressing OCI-AML2 cells (Fig. 1B). Then, flow cytometry analysis using dihydroethidium (DHE) confirmed a remarkable accumulation of cellular ROS in OCI-AML3 cells harboring NPM1-mA, compared with OCI-AML2 cells carrying NPM1-wt (Fig. 1C). Consistently, mitochondrial ROS levels measured by MitoSOX staining were also significantly elevated in OCI-AML3 cells (Fig. 1D). To further evaluate the impact of NPM1-mA on ROS levels, OCI-AML3 cells with stable NPM1 knockdown were generated (Fig. S1C and D). The results showed that NPM1-mA depletion resulted in a remarkable reduction in both intracellular ROS and mitochondrial ROS levels (Fig. 1E and F). Conversely, the overexpression of NPM1-mA significantly increased intracellular ROS and mitochondrial ROS levels, whereas the overexpression of NPM1-wt did not (Fig. 1G and H). These observations indicate that oxidative stress and ROS accumulation are enhanced in NPM1-mutated leukemia cells.

NRF2 is significantly augmented and associated with poor prognosis in NPM1-mutated AML

Given the critical role of NRF2 in defending against cellular oxidative stress, we hypothesized that NRF2 may be augmented to sense ROS in NPM1-mutated cells. To test this, we first analyzed gene expression profiles from public databases (GSE68466 and TCGA) and found that the transcriptional levels of *NRF2 (NFE2L2)* were significantly elevated in the NPM1-mutated AML patients, compared to NPM1-unmutated AML patients (Fig. 2A and B). Furthermore, Kaplan-Meier analysis using the KM plotter online tool revealed that high *NRF2 (NFE2L2)* expression was associated with significantly worse overall survival and post-progression survival in NPM1-mutated AML patients compared to those with low *NRF2* expression (Fig. 2C). Then, the *NRF2* transcripts levels in leukemia blasts cells derived from AML patients was assessed. The results showed that NRF2 was dramatically upregulated in NPM1-mutated AML patients ($n = 5$) relative to NPM1-unmutated AML patients ($n = 11$) (Fig. 2D). Furthermore, we detected NRF2 expression across a panel of human AML cell lines. The qRT-PCR analysis demonstrated that *NRF2* mRNA levels were preferentially higher in the OCI-AML3 cells compared to other leukemia cells without *NPM1* mutations (Fig. 2E). Consistently, increased NRF2 protein levels were also observed in OCI-AML3 cells (Fig. 2F). Notably, the immunofluorescence staining showed that NRF2 was predominantly in the nucleus in OCI-AML3 cells while mainly in the cytoplasm in OCI-AML2 cells (Fig. 2G). Given that *NPM1* mutations are recognized as initiating lesions in AML [34], we investigated whether NPM1-mA contributes to the regulation of NRF2 expression. Depletion of NPM1-mA significantly reduced both NRF2 mRNA and protein levels (Fig. 2H and I). In contrast, NPM1-mA overexpression increased both NRF2 mRNA and protein levels, while NPM1-wt overexpression had no such effect (Fig. 2L and M). Furthermore, subcellular fractionation analysis indicated that the nuclear NRF2 protein levels were decreased in the NPM1-mA-silenced OCI-AML3 cells (Fig. 2J). Conversely, the nuclear NRF2 protein levels were elevated in the NPM1-mA-enforced OCI-AML2 cells compared to that in the NPM1-wt-enforced cells (Fig. 2N). Consistently, immunofluorescence staining confirmed that *NPM1* mutation induced constitutive nuclear localization of NRF2 in leukemia cells (Fig. 2K and O). Collectively, these findings demonstrate that NPM1-mutated leukemia cells exhibit both elevated expression and nuclear localization of NRF2.

NRF2 is upregulated by FTO via m^{6}A RNA demethylation

Next, we investigated the underlying mechanism for the elevated NRF2 expression in NPM1-mutated AML cells. Given that *NPM1* mutations have been reported to stabilize m^{6}A demethylase FTO to participate in transcriptional regulation [35, 36], we examined whether NRF2 expression is regulated by FTO through m^{6}A modification in NPM1-mutated leukemia cells (Fig. 3A). First, several m^{6}A methylated sites within *NRF2(NFE2L2)* mRNA were predicted utilizing the sequence-based RNA adenosine methylation site predictor (SRAMP) (Fig. 3B). Then the correlation analysis between *FTO* and *NRF2(NFE2L2)* expression in AML patients, performed using GEPIA, revealed a positive association (Fig. 3C). Subsequently, we observed that interference with FTO expression decreased NRF2 mRNA and protein levels (Fig. 3D and E), while FTO overexpression increased NRF2 mRNA and protein levels (Fig. 3F and G). Moreover, the treatment of OCI-AML3 cells with meclofenamic acid (MA) and FB23-2, two selective inhibitors of FTO enzyme activity decreased *NRF2* mRNA levels (Fig. 3H). RNA-binding protein immunoprecipitation (RIP) assays was used to confirmed the interaction between FTO protein and *NRF2* mRNA (Fig. 3I). Methylated RNA immunoprecipitation (MeRIP) assays showed the increased m^{6}A modification levels of *NRF2* mRNA following FTO depletion (Fig. 3J). Additionally, mRNA stability assays demonstrated that both FTO knockdown

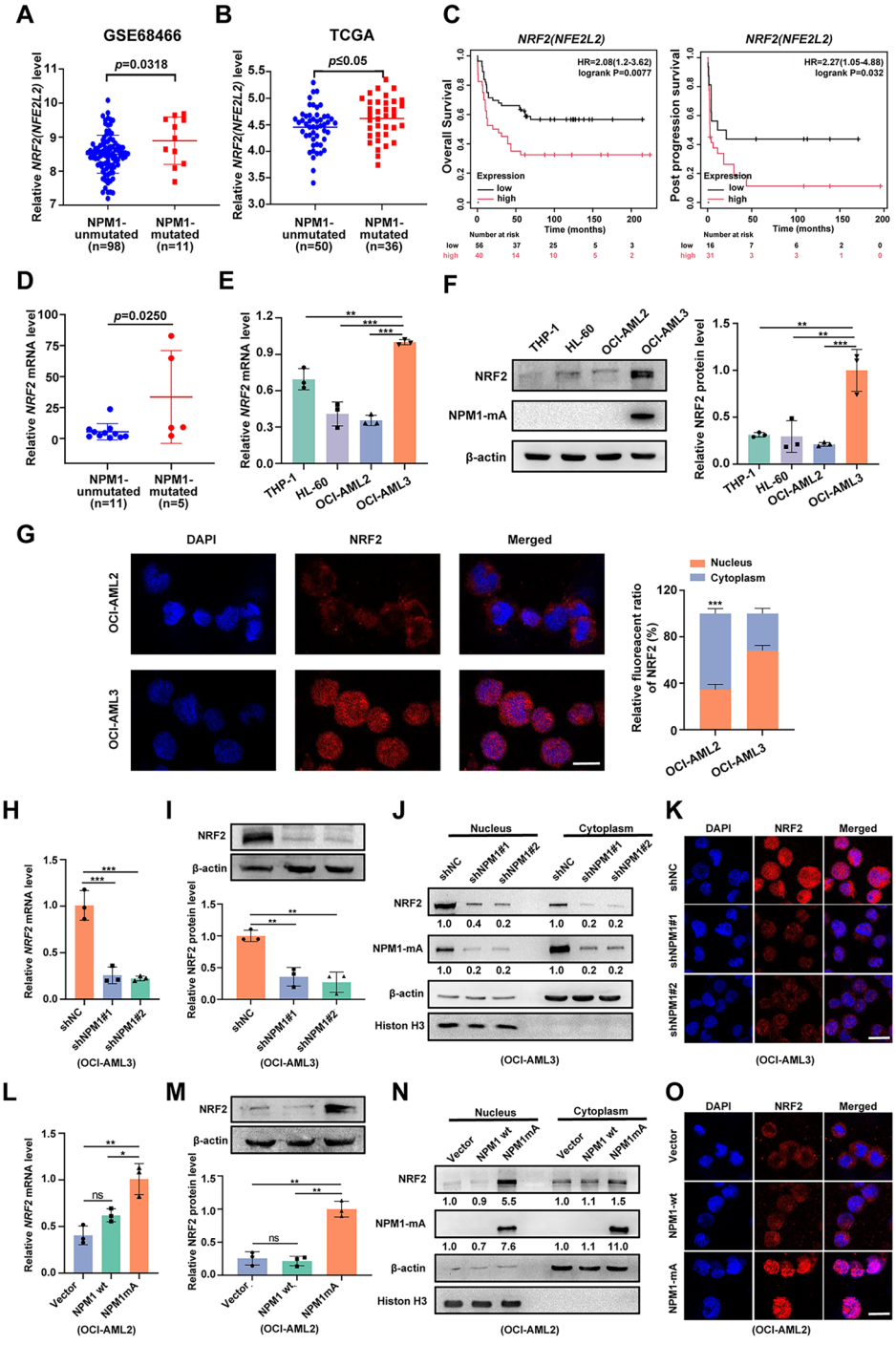

Fig. 2 Antioxidant regulator NRF2 is aberrantly expressed and correlated with worse prognosis in NPM1-mutated AML. **(A, B)** The transcript levels of *NRF2 (NFE2L2)* in NPM1-mutated AML cases compared to NPM1-unmutated AML cases from GSE68466 **(A)** and TCGA **(B)** databases. **(C)** Overall survival and Post progression survival based on high-NRF2 (NFE2L2) or low-NRF2 (NFE2L2) in primary NPM1-mutated AML samples from the KM plotter database (http://kmplot.com). **(D, E)** qRT-PCR analysis of relative *NRF2* mRNA expression in primary AML blasts **(D)** and AML cell lines **(E)**. **(F)** Western blot analysis of relative NRF2 protein expression in AML cell lines. **(G)** Immunofluorescence microscopy after staining with NRF2 (red) and DAPI (blue) demonstrated NRF2 expression in OCI-AML3, OCI-AML2 cells. Scale bar: 20 μm. **(H, L)** qRT-PCR analysis of relative *NRF2* mRNA levels in NPM1-mA-silenced OCI-AML3 cells **(H)**, and NPM1-wt-enforced OCI-AML2, NPM1-mA-enforced OCI-AML2 cells **(L)**. **(I, M)** Western blot analysis of relative NRF2 protein levels in NPM1-mA-silenced OCI-AML3 cells (**I**), and NPM1-wt-enforced OCI-AML2, NPM1-mA-enforced OCI-AML2 cells (**M**). **(J, N)** Western blot analysis of cytoplasmic and nuclear NRF2 protein levels in NPM1-mA-silenced OCI-AML3 cells **(J)**, and NPM1-wt-enforced OCI-AML2, NPM1-mA-enforced OCI-AML2 cells **(N)**. β-actin was used as the cytoplasmic control. Histone H3 was used as the nuclear control. **(K, O)** Immunofluorescence microscopy of NRF2 in NPM1-mA-silenced OCI-AML3 cells **(K)**, and NPM1-wt-enforced OCI-AML2, NPM1-mA-enforced OCI-AML2 cells **(O)**. Scale bar: 20 μm. Data were presented as the mean ± SD of three independent experiments. *$p < 0.05$, **$p < 0.01$, ***$p < 0.001$, ns, not significant

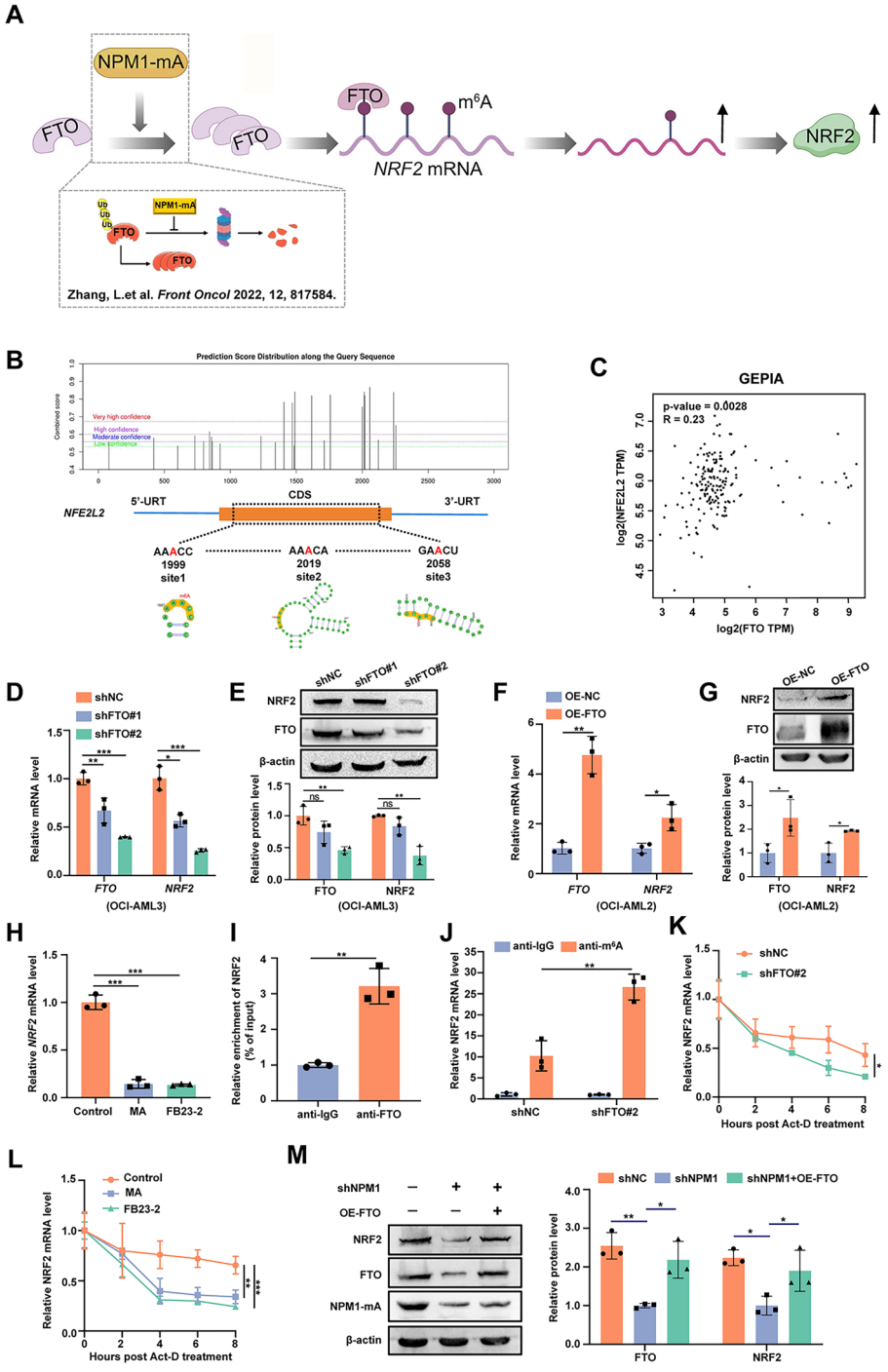

Fig. 3 FTO-mediated m^{6}A modification upregulates NRF2 expression in leukemia cells. **(A)** Schematic diagram of NPM1-mA stabilizing FTO to downregulate m^{6}A abundance and thereby take part in transcriptional regulation. The mechanism by which NPM1-mA stabilizes FTO is as we previously described [35]. Created in https://BioRender.com. **(B)** Prediction score of m^{6}A distribution in *NRF2 (NFE2LE)* mRNA sequence using SRAMP. **(C)** The correlation analysis within *FTO* and *NRF2 (NFE2L2)* expression in AML patients was identified by GEPIA (http://gepia.cancer-pku.cn/index.html). **(D**, **F)** qRT-PCR analysis of relative *FTO* and *NRF2* mRNA levels in FTO-silenced OCI-AML3 cells **(D)**, and FTO-enforced OCI-AML2 **(F)**. **(E**, **G)** Western blot analysis of relative FTO and NRF2 protein levels in FTO-silenced OCI-AML3 cells **(E)**, and FTO-enforced OCI-AML2 **(G)**. **(H)** qRT-PCR analysis of *NRF2* mRNA levels after silencing FTO and inhibiting FTO activity treated by 20 μM FB23-2 and 50 μM MA for 24 h in OCI-AML3 cells. **(I)** RIP-qPCR assay showed significant binding of FTO to *NRF2* mRNA. **(J)** m^{6}A RIP assay showed that knockdown of FTO significantly increased the level of m^{6}A modification of *NRF2* mRNA in OCI-AML3 cells. **(K)** RNA stability assay showed that knockdown of FTO decreased the stability of *NRF2* mRNA after OCI-AML3 cells were treated with 5 μg/mL of Act-D for 0, 2, 4, 6 and 8 h. **(L)** RNA stability assay showed that inhibition of FTO decreased the stability of *NRF2* mRNA after OCI-AML3 cells were treated with 5 μg/mL of Act-D for 0, 2, 4, 6 and 8 h. **(M)** Western blot analysis of relative FTO and NRF2 protein levels in NPM1-mA-silenced OCI-AML3 cells following FTO overexpression. Data were presented as the mean ± SD of three independent experiments. *$p < 0.05$, **$p < 0.01$, ***$p < 0.001$, ns, not significant

and activity inhibition could decrease the stability of *NRF2* mRNA (Fig. 3K and L). Finally, a rescue experiment was conducted to determine whether FTO mediates the NPM1-mA-dependent upregulation of NRF2. The data demonstrated that NPM1-mA knockdown reduced NRF2 protein levels, and then these changes were subsequently restored by FTO overexpression (Fig. 3M). All the above results suggest that NRF2 is upregulated by FTO in a m^6A-depedent manner in AML cells with *NPM1*-mutations.

NRF2 drives downstream target ME1 to promote redox homeostasis and cell survival

To explore the potential mechanisms by which NRF2 contributes to redox homeostasis in leukemia, we performed Kaplan-Meier analysis based on the expression of several antioxidant genes known to be transcriptional targets of NRF2, including *ME1*, *HO1*, *NQO1*, *GCLC*, and *GCLM* [9]. The results showed that high *ME1* expression predicted poor overall survival, whereas the other genes did not exhibit similar prognostic value in NPM1-mutated AML patients (Fig. 4A and B, Fig. S2). Moreover, the *ME1* mRNA was the most significantly downregulated transcript among these genes in NRF2-silenced OCI-AML3 cells (Fig. 4C, Fig. S3). Based on these findings, we focused on ME1, an NADPH-producing enzyme, and further explored its expression and function in leukemia. Western blotting revealed the higher ME1 protein levels in OCI-AML3 cells compared to other leukemia cell lines (Fig. S4A). Then we transfected the siRNA targeting ME1 into OCI-AML3 cells (Fig. S4B and C) and verified that ME1 depletion markedly decreased the intracellular NADPH/$NADP^+$ ratio, increased ROS levels, repressed cell proliferation and promoted apoptotic changes in OCI-AML3 cells (Fig. 4D-G). We next aimed to confirm the regulatory role of NRF2 on ME1 in leukemia. As the result shown, a positive correlation between *NRF2(NFE2L2)* and *ME1* expression was observed in both AML patient samples and AML cell lines (Fig. S5A and B). Western blotting analysis demonstrated that NRF2 depletion markedly reduced ME1 protein expression (Fig. 4H). Since ME1 exerts its antioxidant effects through its enzymatic function, we also assessed ME1 enzymatic activity and found that NRF2 knockdown significantly diminished its activity (Fig. 4I). To determine whether ME1 is a direct downstream target gene of NRF2, we performed a ChIP assay and confirmed that NRF2 directly binds to the antioxidant response elements (AREs) within the ME1 promoter region (Fig. 4J and K). Furthermore, we proceeded to perform ChIP assays in NPM1-mA-enforced cells to probe the role of NRF2-mediated activation of ME1 in leukemia cells with *NPM1* mutation. The results showed that NPM1-mA-enforced cells exhibit more efficient NRF2 binding at the ME1 gene promoter compared to NPM1-wt-enforced cells (Fig. 4L, Fig. S5C). Finally, the rescue experiments showed that NPM1-mA-overexpressing cells displayed elevated ME1 mRNA, protein expression, and enzymatic activity, and then these effects were reversed upon NRF2 knockdown (Fig. 4M-O). Collectively, these results indicate that NRF2/ME1 antioxidant program is activated to promote redox balance and cell survival in NPM1-mutated leukemia cells.

Targeting NRF2 genetically or Pharmacologically disrupts redox homeostasis and induces leukemia cell death

To examine the antioxidant role of NRF2 in NPM1-mutated leukemic cells, we first assessed the redox alterations in NRF2-silenced OCI-AML3 cells. The results demonstrated that NRF2 knockdown significantly reduced the intracellular NADPH/$NADP^+$ ratio (Fig. 5A). Correspondingly, cytoplasmic ROS levels were markedly elevated following NRF2 depletion (Fig. 5B). Notably, CCK-8 assays showed that NRF2 deficiency impaired cell proliferation (Fig. 5C). In addition, NRF2 knockdown increased proportion of apoptotic cells (Fig. 5D). Consistently, pharmacological inhibition of NRF2 using ML385 led to decreased ME1 protein expression and enzymatic activity (Fig. 5E and F), reduced NADPH/$NADP^+$ ratio (Fig. 5G), increased ROS levels (Fig. 5H), impaired cell viability (Fig. 5I), and elevated apoptosis (Fig. 5J). These results demonstrate that both genetic suppression and pharmacologic inhibition of NRF2 result in exacerbated oxidative damage and further cause leukemia cell death.

ML385 cooperates with venetoclax to reduce the viability and induce the cell death of leukemia cells in vitro

Then, we conducted dose-response viability assays in OCI-AML3 cells by combining ML385 with several clinically available drugs, including venetoclax (VEN), cytarabine (AraC), and daunorubicin (DNR) (Fig. 6A). Notably, ML385 exhibited strong synergy with the BCL2 inhibitor VEN in OCI-AML3 cells (Fig. 6B). In addition, CCK-8 assays showed that ML385 acted synergistically with VEN to induce cell death in both OCI-AML3 cells and primary leukemia blasts (Fig. 6C and D). To quantify the interaction, the synergy scores for ML385 and VEN combination were calculated using a dose-response matrix in SynergyFinder (https://synergyfinder.fimm.fi) (Fig. 6E and F). The highest single agent (HSA) synergy scores were 18.78 for OCI-AML3 cells and 15.41 for primary blasts, indicating strong synergistic effects (Fig. 6G and H, HSA scores > 10 suggest synergy, while scores < -10 suggest antagonism). Furthermore, compared to either agent alone, the ML385/VEN combination substantially increased apoptosis in AML cells (Fig. 7A and B). Moreover, the combination treatment upregulated the levels of apoptosis-related proteins BAX and Cleaved CASP3,

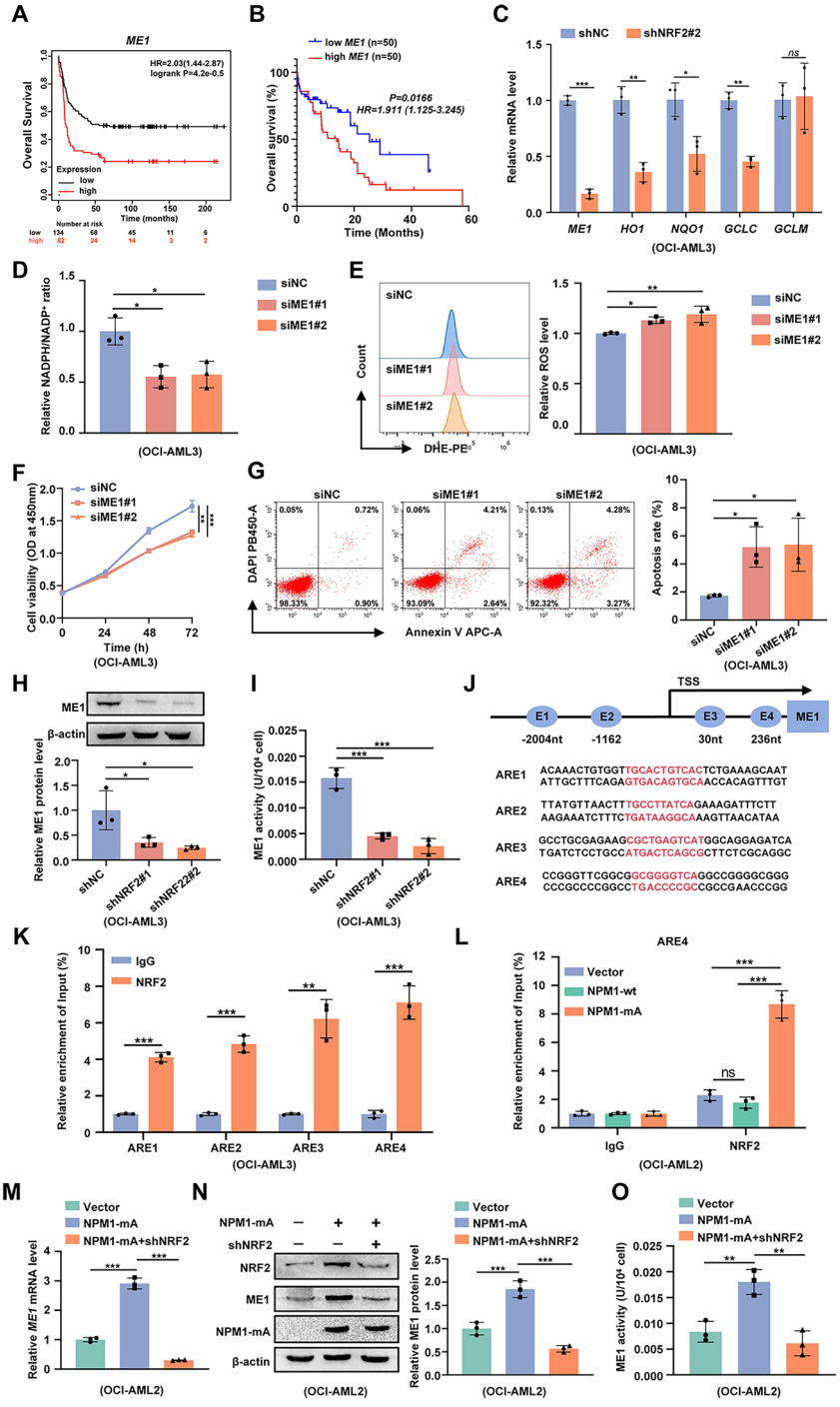

Fig. 4 NRF2/ME1 antioxidant program is activated to promote redox homeostasis and leukemia cell survival. (**A**, **B**) Overall survival based on high-ME1 or low-ME1 in primary NPM1-mutated AML samples from the KM plotter (**A**) and beat-AML (**B**) database. (**C**) qRT-PCR analysis of antioxidative genes downstream of NRF2 in NRF2-knockdown OCI-AML3 cells. (**D**) Measurement of NADPH/NADP$^+$ ratio in OCI-AML3 cells transfected with siME1. (**E**) Flow cytometry analysis of superoxide level using DHE staining in OCI-AML3 cells transfected with siME1. (**F**) CCK-8 assay of cell proliferation activity in siME1 transduced OCI-AML3 cells. (**G**) Flow cytometry analysis of cell apoptosis in siME1 transduced OCI-AML3 cells. (**H**) Western blot analysis of ME1 protein levels in NRF2-knockdown OCI-AML3 cells. **(I)** Measurement of ME1 activity in NRF2-knockdown OCI-AML3 cells. **(J)** Schematic diagram of four antioxidant response elements (AREs) in the promoter region of ME1 (−2004, −1162, +30, and +236 referenced to the transcription start site [TSS]). **(K)** Relative enrichment of NRF2 on the ARE4 of the ME1 promoter was measured by ChIP. **(L)** Relative enrichment of NRF2 on the ME1 promoter was measured by ChIP in NPM1-wt-enforced cells and NPM1-mA-enforced cells. **(M)** qRT-PCR analysis of relative *ME1* mRNA levels in NPM1-mA-enforced OCI-AML2 cells following NRF2 knockdown. **(N)** Western blot analysis of relative ME1 protein levels in NPM1-mA-enforced OCI-AML2 cells following NRF2 knockdown. **(O)** Measurement of ME1 activity in NPM1-mA-enforced OCI-AML2 cells following NRF2 knockdown. Data were presented as the mean ± SD of three independent experiments. *$p < 0.05$, **$p < 0.01$, ***$p < 0.001$, ns, not significant

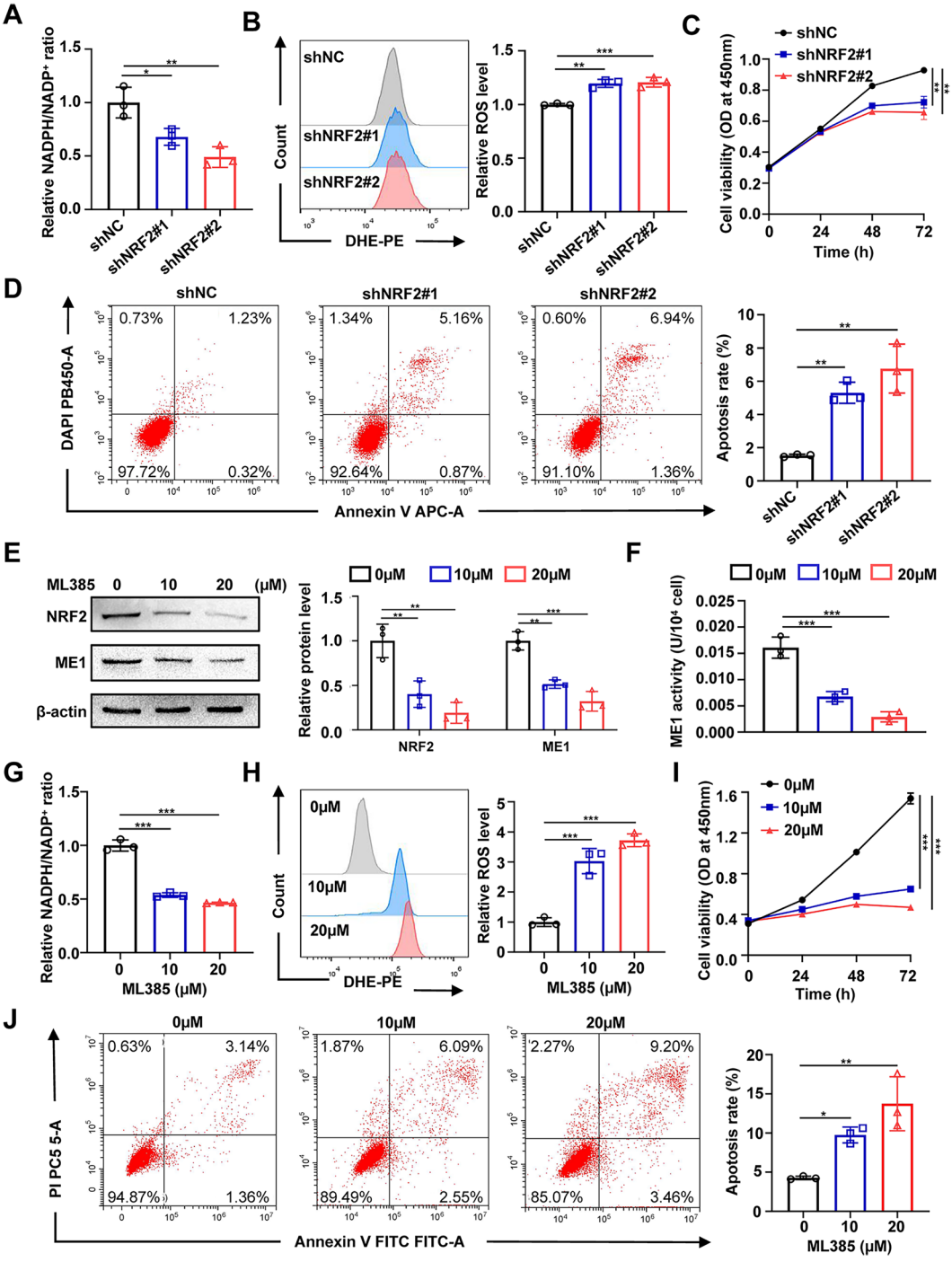

Fig. 5 Genetic and pharmacological inhibition of NRF2 trigger oxidative stress and induce leukemia cell death. **(A)** Measurement of NADPH/NADP$^+$ ratio in NRF2-silenced OCI-AML3 cells. **(B)** Flow cytometry analysis of superoxide level using DHE staining in NRF2-silenced OCI-AML3 cells. **(C)** CCK-8 assay of cell proliferation activity in NRF2-silenced OCI-AML3 cells. **(D)** Flow cytometry analysis of cell apoptosis in NRF2-silenced OCI-AML3 cells. **(E)** Western blot analysis of relative NRF2 and ME1 protein levels in OCI-AML3 cells treated with 0, 10, 20 μM ML385 for 72 h. **(F)** Measurement of ME1 activity in OCI-AML3 cells treated with 0, 10, 20 μM ML385 for 72 h. **(G)** Measurement of NADPH/NADP$^+$ ratio in OCI-AML3 cells treated with 0, 10, 20 μM ML385 for 72 h. **(H)** Flow cytometry analysis of superoxide level using DHE staining in OCI-AML3 cells treated with 0, 10, 20 μM ML385 for 72 h. **(I)** CCK-8 assay of cell proliferation activity in OCI-AML3 cell with 0, 10, 20 μM ML385 for 0, 24, 48, 72 h. **(J)** Flow cytometry analysis of cell apoptosis in OCI-AML3 cells treated with 0, 10, 20 μM ML385 for 72 h. Data were presented as the mean ± SD of three independent experiments. *$p < 0.05$, **$p < 0.01$, ***$p < 0.001$

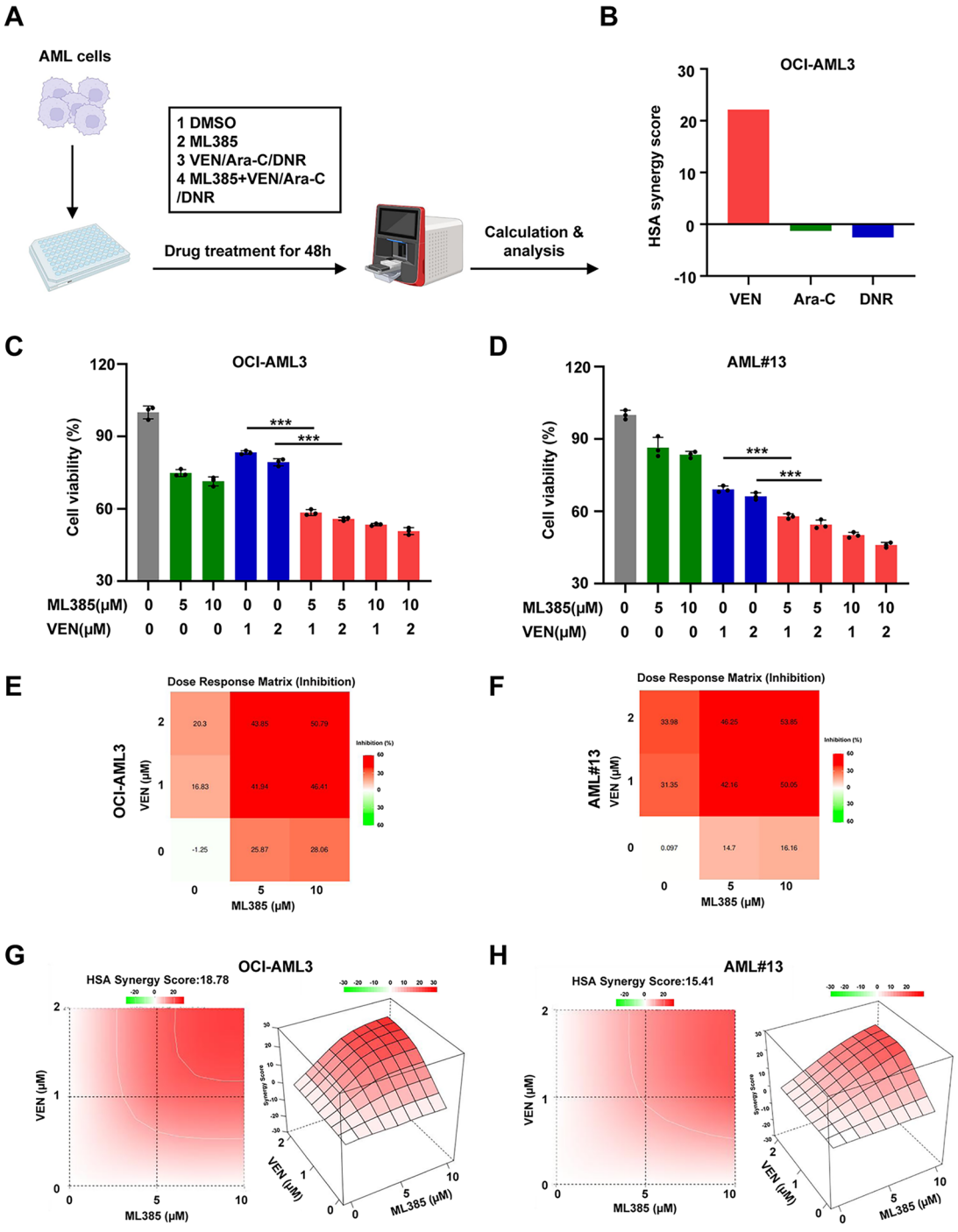

Fig. 6 ML385 cooperates with VEN to reduce the viability of AML cells. **(A)** The schematic depiction of experiments about drug treatment. Created in https://BioRender.com. **(B)** HSA synergy scores of ML385 combination with indicated drugs, including VEN (2μM), Ara-C (500nM) and DNR (50nM) in OCI-AML3 cells for 48 h. HSA scores greater than 10 suggest synergy, scores less than − 10 suggest an antagonistic effect, scores between − 10 and 10 suggest addition effect. **(C**, **D)** CCK-8 assay of cell viability in OCI-AML3 **(C)** or AML#13 **(D)** cells treated with ML385 and VEN, alone or in combination for 48 h. **(E**, **F)** Dose-response matrix of combination response of ML385 + VEN for 48 h in OCI-AML3 cells **(E)** or AML#13 cells **(F)**. **(G**, **H)** Calculation of HSA synergy scores and visualization of synergy maps by SynergyFinder in OCI-AML3 cells **(G)** or AML#13 **(H)** treated with ML385 + VEN for 48 h. Data were presented as the mean ± SD of three independent experiments. *$p < 0.05$, **$p < 0.01$, ***$p < 0.001$

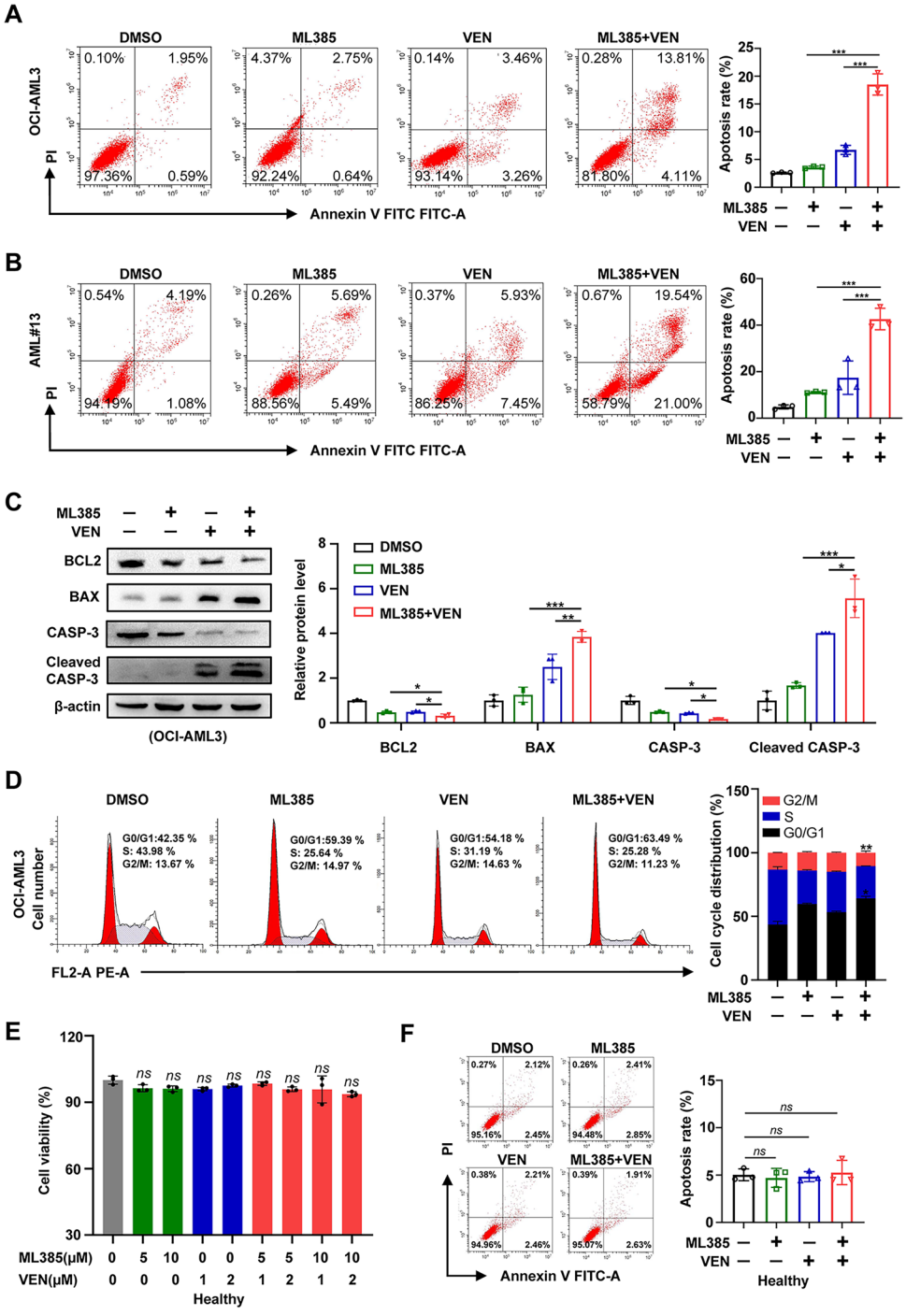

Fig. 7 ML385 cooperates with VEN to induce the cell death of AML cells. **(A, B)** Flow cytometry analysis of cell apoptosis in OCI-AML3 cells **(A)** and AML#13 cells **(B)** treated with ML385 and VEN, alone or in combination for 48 h. **(C)** Western blot analysis of these apoptosis related proteins in OCI-AML3 cells treated with ML385 and VEN, alone or in combination for 48 h. **(D)** Flow cytometric analysis of cell cycle distribution in OCI-AML3 cells treated with ML385 and VEN, alone or in combination for 48 h. **(E, F)** CCK-8 assay of cell viability **(E)** and flow cytometry analysis of cell apoptosis **(F)** in the mononuclear cells from healthy donors. Data were presented as the mean ± SD of three independent experiments. *$p < 0.05$, **$p < 0.01$, ***$p < 0.001$

while downregulating BCL2 and full-length CASP3 in OCI-AML3 cells (Fig. 7C). Additionally, the combination treatment resulted in the arrest of the cell cycle of OCI-AML3 cells in the G0/G1 phase (Fig. 7D). Besides, the treatment with ML385, VEN, or their combination did not significantly affect the cell viability of normal blood cells from healthy donors (Fig. 7E and F). Taken together, these data suggested that co-treatment with ML385 and VEN exerts a strong synergism anti-leukemic effect in vitro.

The combination of ML385 and venetoclax reduces leukemia burden and prolongs survival in vivo

To evaluate whether the anti-leukemic effects of ML385, VEN, or their combination observed in vitro could be replicated in vivo, we established a cell line-derived xenograft (CDX) model by injecting OCI-AML3 cells into NOD/SCID mice. Three weeks post-injection, mice were treated with ML385, VEN, or their combination for 4 weeks (Fig. 8A). Flow cytometry analysis revealed that the percentage of human CD45-positive ($hCD45^+$) cells in the bone marrow (BM) was significantly reduced in the combination group compared to the ML385 or VEN monotherapy groups (Fig. 8B). In addition, combination treatment markedly reduced spleen and liver weights, as well as leukemic infiltration in both organs (Fig. 8C-F). Wright's staining showed significantly fewer leukemic cells in the bone marrow of the combination group compared to either monotherapy group (Fig. 8G). Moreover, the treatment with a single agent (ML385) led to a reduction in leukemic burden within the bone marrow, liver, and spleen of mice (Fig. 8B-G). In addition, western blot analysis sfurther demonstrated that the combination therapy increased expression of the pro-apoptotic proteins BAX and cleaved CASP3, while decreasing levels of BCL2 and full-length CASP3 (Fig. 8H). Kaplan-Meier survival curves demonstrated that ML385 and VEN strongly synergized to extend survival in xenograft models (Fig. 8I). In addition, the analysis of serum samples for blood biochemical markers was performed and revealed no evident signs of toxicity, indicating that the mice tolerated the therapy (Fig. S6). Collectively, these results suggest that ML385 synergizes with venetoclax-based chemotherapy *in vivio*.

Discussion

Extensive evidence has established that oxidative stress regulation plays a critical role in both cancer progression and responsiveness to anti-tumor therapies [37]. However, the redox status of NPM1-mutated AML and the role of the reprogrammed ROS metabolism in anti-leukemic therapy remain insufficiently defined. Herein, our data demonstrate that NPM1-mutated AML cells accumulate ROS and exhibit elevated NRF2 expression, and the high NRF2 levels are at least partially upregulated by FTO through m^6A modification. Functionally, NRF2 maintains redox homeostasis and supports cell survival by activating the NADPH-producing enzyme ME1. Importantly, NRF2 inhibition alone or in combination with the targeted agent venetoclax induces leukemia cell death (Fig. 9).

In the current study, we found that NPM1-mutated leukemia exhibits a propensity toward oxidative stress, as overexpression of mutant NPM1 is closely associated with elevated levels of both cellular and mitochondrial ROS. Indeed, our findings are supported by previous studies indicating that leukemia cells with *NPM1* mutations are regarded to carry more ROS due to altered mitochondrial functions and metabolism reprogramming [14, 38]. Though ROS can promote tumorigenesis, excessive ROS levels not only inhibit cell proliferation but also trigger cell death pathways [39]. To counteract this, multiple tumor cells accrete genetic alterations that enhance antioxidant defenses to prevent ROS from reaching cytotoxic levels [40]. Within the network of antioxidant transcription factors, NRF2 has been proposed to act as a "flood gate" regulator, maintaining redox balance under stress, while other numbers of the network become activated only when NRF2-dependent antioxidant capacity is overwhelmed [16]. In our research, we analyzed *NRF2* mRNA levels in NPM1-mutated AML patients using public databases, and further assessed NRF2 expression and subcellular location in leukemia cell lines. These results revealed the relatively high expression and predominant nuclear localization of NRF2 in NPM1-mutated leukemia cells. Notably, Milkovic L et al. [41] have reported that NRF2 governs the cellular response to oxidative stress across multiple cancer types. Moreover, sustained NRF2 overexpression and constitutive nuclear activation have been linked to the malignant phenotype and drug resistance in AML [42]. Our survival analysis using the KM plotter tool further showed that high *NRF2* expression is associated with poor prognosis in NPM1-mutated AML, consistent with a prior study demonstrating that AML patients with elevated NRF2 levels exhibit worse clinical outcomes [43]. In addition to NRF2, many transcription factors—such as NF-kB, HIF-1α, FOXO, PGC-1α—have also been reported be activated by ROS, thereby contributing to redox regulation and carcinogenesis [16, 44, 45]. Further studies are warranted to investigate whether these or other antioxidant regulators are similarly activated and contribute to redox homeostasis in NPM1-mutated leukemia.

We further investigated the molecular mechanism underlying the elevated expression of NRF2 in NPM1-mutated leukemia. Our results revealed that knockdown of NPM1-mA decreased NRF2 mRNA and protein levels, whereas enforced expression of NPM1-mA had the

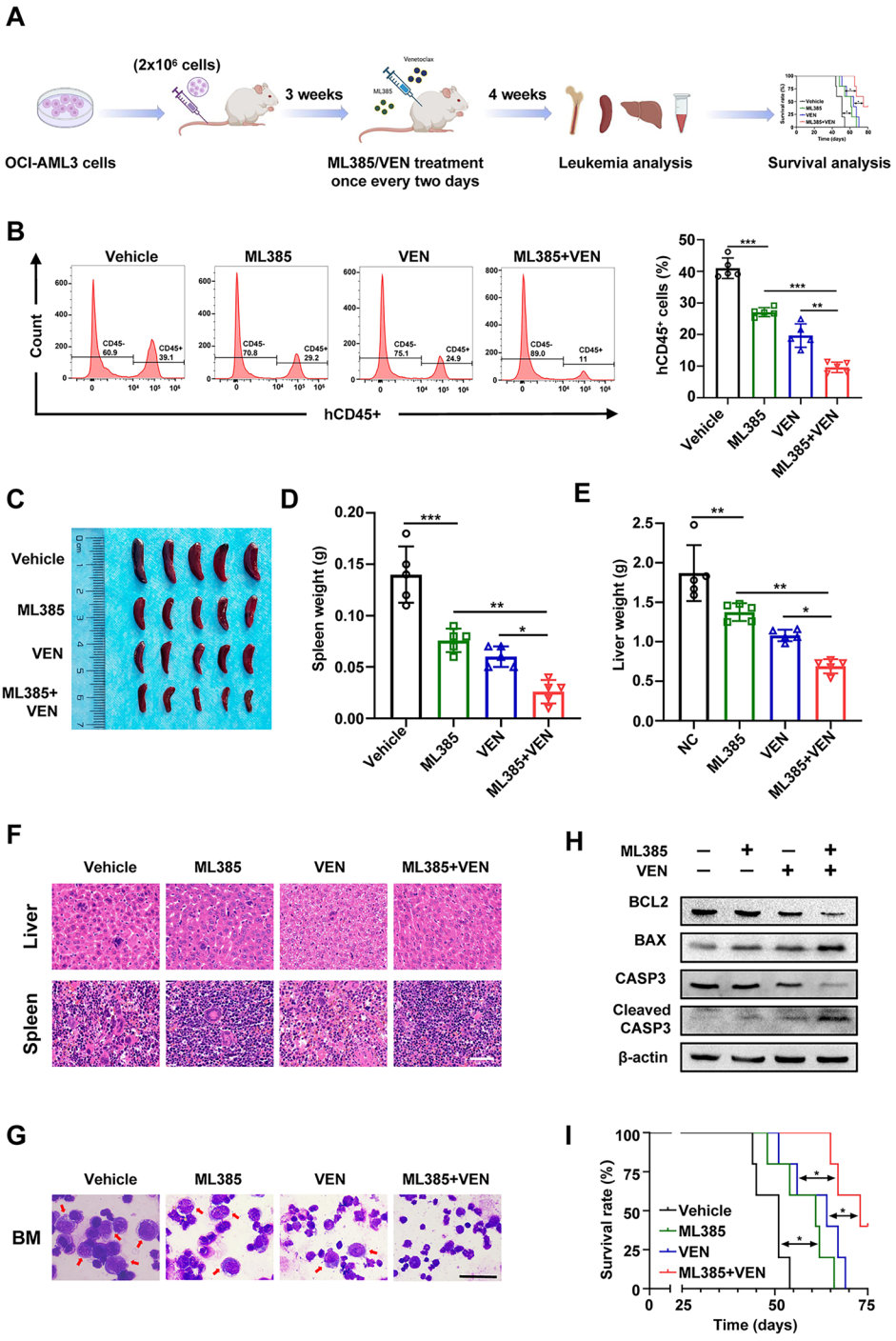

Fig. 8 ML385 shows anti-leukemic activity in a CDX model both as a single agent and in combination with venetoclax. **(A)** Establishment and treatment schedule of CDX mice model via intravenous injection OCI-AML3 cells. **(B)** Flow cytometric analysis of human CD45$^+$ cells percentage in the bone marrow (BM). **(C)** Spleen images of the mice after treatment. **(D, E)** The weight of the spleens **(D)** and livers **(E)** of the mice after treatment. **(F)** Representative H&E staining images of mice liver and spleen. Scale bar: 50 μm. **(G)** Wright's staining of immature cells from bone marrow (BM). Scale bar: 50 μm. **(H)** Western blot analysis of apoptosis related proteins. **(I)** Kaplan-Meier analysis of the survival curves of the mice in each group. Data were presented as the mean ± SD ($n = 5$). *$p < 0.05$, **$p < 0.01$, ***$p < 0.001$

opposite effect. NPM1-mA functions as a chaperone protein and is not capable of directly regulating gene transcription [46], but has been shown to stabilize the m^{6}A demethylase FTO and participate in in transcriptional regulation in our previous studies [35, 36]. Thus, we speculated that NRF2 expression may be partially regulated by FTO-mediated m^{6}A modification in NPM1-mutated leukemia cells. In the present study, we found that

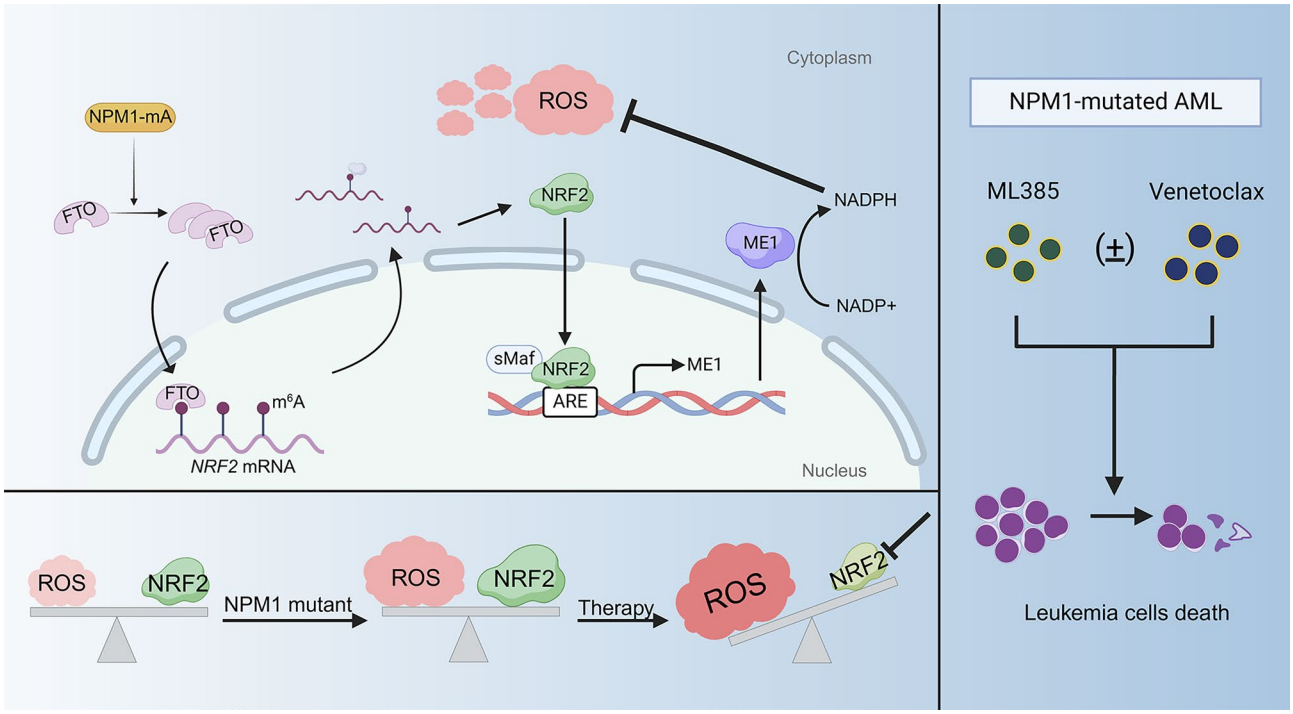

Fig. 9 Schematic diagram describing the functional significance of NRF2/ME1 antioxidant pathway and the novel therapy strategy targeting NRF2 in NPM1-mutated leukemia. NRF2 is modulated by FTO-mediated m^{6}A demethylation and promotes ME1 expression by NADPH generation to maintain redox homeostasis. NRF2 inhibition alone or in combination with venetoclax could be used to kill leukemia cells. Created in BioRender (https://BioRender.com/t85t921)

FTO knockdown decreased, and FTO overexpression increased NRF2 expression in leukemia cells. Furthermore, treatment of OCI-AML3 cells with two FTO inhibitors, MA and FB23-2, led to downregulation of *NRF2* mRNA levels. RIP experiment confirmed the interaction between *NRF2* mRNA and FTO protein. Additionally, MeRIP and RNA stability assays demonstrated that FTO upregulated NRF2 expression by reducing the m^{6}A methylation level of *NRF2* mRNA. Previous studies have proposed other regulatory mechanisms of NRF2 expression. For instance, the methyltransferase METTL4 was shown to induce the m^{6}A modification of *NRF2* mRNA in acute lung injury [47]. Besides, the deacetylase SIRT1 was identified as an upstream regulator of NRF2 via activation of PGC-1α in nonchemical models of liver perturbation [48]. Recently, a study revealed that the long non-coding RNA SNAI3-AS1 decreases *NRF2* mRNA stability by perturbing the m^{6}A-dependent recognition of *NRF2* transcripts in glioma [49]. Future studies are needed to explore whether additional regulatory mechanisms are involved in NRF2 expression in leukemia.

Next, we screened for downstream target genes of NRF2 using the qPCR and bioinformatics analyses, and identified the antioxidant enzyme ME1 as a candidate of interest. The data in our study showed that NRF2 knockdown led to the most pronounced reduction in *ME1* mRNA levels in OCI-AML3 cells. Furthermore, ChIP assays confirmed ME1 is a direct transcriptional target of NRF2. NRF2 inhibition (genetically or pharmacologically using ML385) decreased ME1 expression and enzymatic activity. In addition, survival analysis showed that high *ME1* expression was related to poor prognosis in AML patients. Collectively, these findings indicate that ME1 is a key downstream effector of NRF2 in NPM1-mutated AML. ME1 is known to regulate NADPH homeostasis, thereby contributing to redox balance [50], and to support reductive biosynthesis [51]. Notably, Lee et al. [33] have demonstrated that NRF2 transcriptionally activates ME1 to generate NADPH in response to further ROS insult in hepatocellular carcinoma cells. In our study, either genetic or pharmacological inhibition of NRF2 reduced the NADPH/NADP$^+$ ratio and increased intracellular ROS levels, ultimately inducing leukemia cell death. These results highlighted the critical role of NRF2/ME1 axis in redox regulation in AML cells with *NPM1* mutation. In addition to NRF2-activated ME1/NADPH axis, previous findings have suggested that NPM1-mutated leukemia may exhibit a specific dependency on ROS scavenging pathways, such as GSH metabolism [532].

Given that NPM1-mutated AML cells develop an addiction to NRF2-governed pathways, targeting NRF2 may offer a personalized therapeutic strategy for NPM1-mutated patients with high NRF2 expression. This study

is the first to demonstrate the potential of the NRF2 inhibitor ML385 as a therapeutic agent for NPM1-mutated AML. In recent years, the precision medicine has been increasingly proposed for AML treatment [53], and a growing body of evidence has indicated that the NRF2 blockade has synergistic toxicity with chemotherapy, thereby improving anti-tumor effects [54–56]. Notably, ML385 has already been reported to increase the effectiveness of the chemotherapy agent doxorubicin (Dox) in Dox-resistant leukemia cells, likely through the mitochondrial-dependent apoptosis pathway [57]. In addition to targeting NRF2, future research will focus on the safety and feasibility of clinically targeting ME1 in NPM1-mutated leukemia.

VEN, a potent and selective BCL2 inhibitor, has demonstrated synergy with azacitidine in AML [58]. Currently, the Food and Drug Administration (FDA) has approved the VEN-based combination regimens for newly diagnosed elderly AML patients who are unfit for intensive chemotherapy [58, 59]. In this work, we validated the combinatorial efficacy of ML385 and VEN in NPM1-mutated leukemia both in vitro and in vivo. Furthermore, we proposed that the higher ROS generation induced by ML385 combined with venetoclax at least partially underlies the fundamental synergistic mechanisms of the combination treatment (Data not shown). Consistently, Yu X et al. [60] have found that ML385 enhances the sensitivity of AML cells to VEN via the ferroptosis pathway. Of course, further work is necessitated to validate the therapeutic strategy in patient-derived xenograft (PDX) models that mimic human NPM1-mutated leukemia.

Conclusion

In summary, we first identified an increased ROS burden in leukemia cells with *NPM1* mutations, along with increased NRF2 expression driven by demethylase FTO-mediated m^6A RNA modification. Furthermore, genetic or pharmacologic blockade of NRF2 disrupted redox homeostasis and impaired cell proliferation. Mechanistically, NRF2 conferred cytoprotective effects by inducing ME1 expression and facilitating ROS scavenging through NADPH production. Importantly, our findings illustrated that targeting the antioxidant pathway represents a promising therapeutic strategy for AML characterized by elevated ROS burden, and may support the development of novel combination therapy.

Abbreviations

NRF2	Nuclear Factor (erythroid-derived 2)-like 2
ME1	Malic Enzyme 1
AML	Acute Myeloid Leukemia
NPM1	Nucleophosmin 1
ROS	Reactive Oxygen Species
FTO	Fat Mass and Obesity-Associated Protein
m^6A	N6-methyladenosine
VEN	Venetoclax
ARE	Antioxidant Response Elements
sMAF	Small Musculoaponeurotic Fibrosarcoma
shRNA	Short Hairpin RNA
GSEA	Gene Set Enrichment Analysis
GO	Gene Ontology
DHE	Dihydroethidium
NPM1-mA	Mutant NPM1 type A
NPM1-wt	Wild-Type NPM1
GSE68466	Gene Expression Omnibus Database Under the Accession Numbers GSE68466
TCGA	The Cancer Genome Atlas
KM plotter	Kaplan-Meier Plotter
SRAMP	Sequence-Based RNA Adenosine Methylation Site Predictor
GEPIA	Gene Expression Profiling Interactive Analysis
MA	Meclofenamic Acid
RIP	RNA-Binding Protein Immunoprecipitation
MeRIP	Methylated RNA Immunoprecipitation
Act-D	Actinomycin D
HO1	Heme Oxygenase 1
NQO1	Quinone Oxidoreductase 1
NADPH	Nicotinamide Adenine Dinucleotide Phosphate Hydrogen
GCLC	Glutamate-Cysteine Ligase Catalytic Subunit
GCLM	Glutamate-Cysteine Ligase Modifier Subunit
CCLE	Cancer Cell Line Encyclopedia
HSA	Highest Single Agent

Supplementary Information

The online version contains supplementary material available at https://doi.org/10.1186/s40170-025-00401-6.

Supplementary Material 1

Acknowledgements

The authors would like to acknowledge the Key Laboratory of Laboratory Medical Diagnostics Designated by the Ministry of Education, College of Laboratory Medicine (Chongqing Medical University, Chongqing, China) for providing the space and equipment for conducting the experiments.

Author contributions

JY, ZH and JR planned and performed experiments; LS, XY, YC and FF analyzed data; JY, XY and YS contributed reagents and other essential material; NW, QLX and WZ organized the figures and wrote the paper; ZL and LZ revised this manuscript. All authors reviewed the manuscript.

Funding

This work was supported by National Natural Science Foundation of China (Grant No: 82072353) to Ling Zhang, the Chongqing Graduate Research and Innovation Project of the Chongqing Education Committee (CYS23351) for Jiayuan Hu and the Research Project of Fuling District of Chongqing City (No. FLKJ, 2024AAN3058).

Data availability

No datasets were generated or analysed during the current study.

Declarations

Ethics approval and consent to participate

Ethical approval was given by the Medical Ethics Committee of Chongqing Medical University. All animal procedures to be employed in the project was approved by Institutional Animal Care and Use of Chongqing Medical University (Approval number: IACUC-CQMU-2025-0338).

Competing interests

The authors declare no competing interests.

Author details
[1]Key Laboratory of Laboratory Medical Diagnostics Designated by the Ministry of Education, College of Laboratory Medicine, Chongqing Medical University, Chongqing 400016, China
[2]Department of Laboratory Medicine, Chongqing University Fuling Hospital, School of Medicine, Chongqing University, Chongqing, China

Received: 29 January 2025 / Accepted: 12 June 2025
Published online: 18 June 2025

References

1. Deschler B, Lübbert M. Acute myeloid leukemia: epidemiology and etiology. Cancer. 2006;107:2099–107.
2. DiNardo CD, Erba HP, Freeman SD, Wei AH. Acute myeloid leukaemia. Lancet. 2023;401:2073–86.
3. Falini B, Martelli MP, Bolli N, Sportoletti P, Liso A, Tiacci E, Haferlach T. Acute myeloid leukemia with mutated nucleophosmin (NPM1): is it a distinct entity? Blood. 2011;117:1109–20.
4. Falini B, Brunetti L, Sportoletti P, Martelli MP. NPM1-mutated acute myeloid leukemia: from bench to bedside. Blood. 2020;136:1707–21.
5. Ranieri R, Pianigiani G, Sciabolacci S, Perriello VM, Marra A, Cardinali V, et al. Current status and future perspectives in targeted therapy of NPM1-mutated AML. Leukemia. 2022;36:2351–67.
6. Becker H, Marcucci G, Maharry K, Radmacher MD, Mrózek K, Margeson D, et al. Favorable prognostic impact of NPM1 mutations in older patients with cytogenetically normal de Novo acute myeloid leukemia and associated gene- and microRNA-expression signatures: a Cancer and leukemia group B study. J Clin Oncol. 2010;28:596–604.
7. Scholl S, Theuer C, Scheble V, Kunert C, Heller A, Mügge LO. Clinical impact of nucleophosmin mutations and Flt3 internal tandem duplications in patients older than 60 year with acute myeloid leukaemia. Eur J Haematol. 2008;80:208–15.
8. Cheung EC, Vousden KH. The role of ROS in tumour development and progression. Nat Rev Cancer. 2022;22:280–97.
9. Sies H, Jones DP. Reactive oxygen species (ROS) as pleiotropic physiological signalling agents. Nat Rev Mol Cell Biol. 2020;21:363–83.
10. Tang X, Fu X, Liu Y, Yu D, Cai SJ, Yang C. Blockade of glutathione metabolism in IDH1-Mutated glioma. Mol Cancer Ther. 2020;19:221–30.
11. Yu D, Liu Y, Zhou Y, Ruiz-Rodado V, Larion M, Xu G, Yang C. Triptolide suppresses IDH1-mutated malignancy via Nrf2-driven glutathione metabolism. Proc Natl Acad Sci USA. 2020;117:9964–72.
12. Liu Y, Lu Y, Celiku O, Li A, Wu Q, Zhou Y, Yang C. Targeting IDH1-Mutated malignancies with NRF2 Blockade. J Natl Cancer Inst. 2019;111:1033–41.
13. Kannan S, Irwin ME, Herbrich SM, Cheng T, Patterson LL, Aitken MJL, et al. Targeting the NRF2/HO-1 antioxidant pathway in FLT3-ITD-Positive AML enhances therapy efficacy. Antioxid (Basel). 2022;11:717.
14. Wu HC, Rérolle D, Berthier C, Hleihel R, Sakamoto T, Quentin S, et al. Actinomycin D targets NPM1c-Primed mitochondria to restore PML-Driven senescence in AML therapy. Cancer Discov. 2021;11:3198–213.
15. Marinho HS, Real C, Cyrne L, Soares H, Antunes F. Hydrogen peroxide sensing, signaling and regulation of transcription factors. Redox Biol. 2014;2:535–62.
16. Hayes JD, Dinkova-Kostova AT, Tew KD. Oxidative stress in Cancer. Cancer Cell. 2020;38:167–97.
17. Hayes JD, Dinkova-Kostova AT. The Nrf2 regulatory network provides an interface between redox and intermediary metabolism. Trends Biochem Sci. 2014;39:199–218.
18. de la Rojo M, Chapman E, Zhang DD. NRF2 and the hallmarks of Cancer. Cancer Cell. 2018;34:21–43.
19. DeNicola GM, Karreth FA, Humpton TJ, Gopinathan A, Wei C, Frese K, et al. Oncogene-induced Nrf2 transcription promotes ROS detoxification and tumorigenesis. Nature. 2011;475:106–9.
20. Suzuki T, Muramatsu A, Saito R, Iso T, Shibata T. Kuwata Ket al. Molecular mechanism of cellular oxidative stress sensing by Keap1. Cell Rep. 2019;28:746–58.
21. Hecht F, Zocchi M, Alimohammadi F, Harris IS. Regulation of antioxidants in cancer. Mol Cell. 2024;84:23–33.
22. Wolowczyk C, Neckmann U, Aure MR, Hall M, Johannessen B, Zhao S, et al. NRF2 drives an oxidative stress response predictive of breast cancer. Free Radic Biol Med. 2022;184:170–84.
23. Zhang Q, Zhang ZY, Du H, Li SZ, Tu R, Jia YF, et al. DUB3 deubiquitinates and stabilizes NRF2 in chemotherapy resistance of colorectal cancer. Cell Death Differ. 2019;26:2300–13.
24. Lu YX, Ju HQ, Liu ZX, Chen DL, Wang Y, Zhao Q, et al. ME1 regulates NADPH homeostasis to promote gastric Cancer growth and metastasis. Cancer Res. 2018;78:1972–85.
25. Singh A, Venkannagari S, Oh KH, Zhang YQ, Rohde JM, Liu L, et al. Small molecule inhibitor of NRF2 selectively intervenes therapeutic resistance in KEAP1-Deficient NSCLC tumors. ACS Chem Biol. 2016;11:3214–25.
26. Kansanen E, Kuosmanen SM, Leinonen H, Levonen AL. The Keap1-Nrf2 pathway: mechanisms of activation and dysregulation in Cancer. Redox Biol. 2013;1:45–9.
27. Jeong EJ, Choi JJ, Lee SY, Kim YS. The effects of ML385 on head and neck squamous cell carcinoma: implications for NRF2 Inhibition as a therapeutic strategy. Int J Mol Sci. 2024;25:7011.
28. Cunningham A, Oudejans LL, Geugien M, Pereira-Martins DA, Wierenga ATJ, Erdem A et al. The nonessential amino acid cysteine is required to prevent ferroptosis in acute myeloid leukemia.blood adv. 2024;8: 56–69.
29. Lachowiez CA, Loghavi S, Kadia TM, Daver N, Borthakur G, Pemmaraju N, et al. Outcomes of older patients with NPM1-mutated AML: current treatments and the promise of venetoclax-based regimens. Blood Adv. 2020;4:1311–20.
30. Stahl M, Menghrajani K, Derkach A, Chan A, Xiao W, Glass J, et al. Clinical and molecular predictors of response and survival following venetoclax therapy in relapsed/refractory AML. Blood Adv. 2021;5:1552–64.
31. Ren J, Tao Y, Peng M, Xiao Q, Jing Y, Huang J, et al. Targeted activation of GPER enhances the efficacy of venetoclax by boosting leukemic pyroptosis and CD8 + T cell immune function in acute myeloid leukemia. Cell Death Dis. 2022;13:915.
32. Ren J, Huang J, Yang Z, Sun M, Yang J, Lin C, et al. Cytoplasmic TP53INP2 acts as an apoptosis partner in TRAIL treatment: the synergistic effect of TRAIL with venetoclax in TP53INP2-positive acute myeloid leukemia. J Exp Clin Cancer Res. 2024;43:176.
33. Lee D, Zhang MS, Tsang FH, Bao MH, Xu IM, Lai RK, et al. Adaptive and constitutive activations of malic enzymes confer liver Cancer multilayered protection against reactive oxygen species. Hepatology. 2021;74:776–96.
34. Falini B, Mecucci C, Tiacci E, Alcalay M, Rosati R, Pasqualucci L, et al. GIMEMA acute leukemia working party. Cytoplasmic nucleophosmin in acute myelogenous leukemia with a normal karyotype. N Engl J Med. 2005;352:254–66.
35. Xiao Q, Lei L, Ren J, Peng M, Jing Y, Jiang X, et al. Mutant NPM1-Regulated FTO-Mediated m6A demethylation promotes leukemic cell survival via PDGFRB/ERK signaling Axis. Front Oncol. 2022;12:817584.
36. Huang J, Sun M, Tao Y, Ren J, Peng M, Jing Y, et al. Cytoplasmic expression of TP53INP2 modulated by demethylase FTO and mutant NPM1 promotes autophagy in leukemia cells. Int J Mol Sci. 2023;24:1624.
37. Gorrini C, Harris IS, Mak TW. Modulation of oxidative stress as an anticancer strategy. Nat Rev Drug Discov. 2013;12:931–47.
38. Erdem A, Marin S, Pereira-Martins DA, Cortés R, Cunningham A, Pruis MG, et al. The glycolytic gatekeeper PDK1 defines different metabolic States between genetically distinct subtypes of human acute myeloid leukemia. Nat Commun. 2022;13:1105.
39. Dixon SJ, Stockwell BR. The role of iron and reactive oxygen species in cell death. Nat Chem Biol. 2014;10:9–17.
40. Harris IS, DeNicola GM. The complex interplay between antioxidants and ROS in Cancer. Trends Cell Biol. 2020;30:440–51.
41. Milkovic L, Zarkovic N, Saso L. Controversy about Pharmacological modulation of Nrf2 for cancer therapy. Redox Biol. 2017;12:727–32.
42. Rushworth SA, Zaitseva L, Murray MY, Shah NM, Bowles KM, MacEwan DJ. The high Nrf2 expression in human acute myeloid leukemia is driven by NF-κB and underlies its chemo-resistance. Blood. 2012;120:5188–98.
43. Liu X, Zhong S, Qiu K, Chen X, Wu W, Zheng J, et al. Targeting NRF2 uncovered an intrinsic susceptibility of acute myeloid leukemia cells to ferroptosis. Exp Hematol Oncol. 2023;12:47.
44. Rodriguez-Colman MJ, Dansen TB, Burgering BMT. FOXO transcription factors as mediators of stress adaptation. Nat Rev Mol Cell Biol. 2024;25:46–64.
45. Guo X, Jiang Q, Tuccitto A, Chan D, Alqawlaq S, Won GJ, Sivak JM. The AMPK-PGC-1α signaling axis regulates the astrocyte glutathione system to protect against oxidative and metabolic injury. Neurobiol Dis. 2018;113:59–69.
46. Heath EM, Chan SM, Minden MD, Murphy T, Shlush LI, Schimmer AD. Biological and clinical consequences of NPM1 mutations in AML. Leukemia. 2017;31:798–807.

47. Sang A, Zhang J, Zhang M, Xu D, Xuan R, Wang S, et al. METTL4 mediated-N6-methyladenosine promotes acute lung injury by activating ferroptosis in alveolar epithelial cells. Free Radic Biol Med. 2024;213:90–101.
48. Kulkarni SR, Donepudi AC, Xu J, Wei W, Cheng QC, Driscoll MV, et al. Fasting induces nuclear factor E2-related factor 2 and ATP-binding cassette transporters via protein kinase A and Sirtuin-1 in mouse and human. Antioxid Redox Signal. 2014;20:15–30.
49. Zheng J, Zhang Q, Zhao Z, Qiu Y, Zhou Y, Wu Z, et al. Epigenetically silenced LncRNA SNAI3-AS1 promotes ferroptosis in glioma via perturbing the m6A-dependent recognition of Nrf2 mRNA mediated by SND1. J Exp Clin Cancer Res. 2023;42:127.
50. Tao R, Zhao Y, Chu H, Wang A, Zhu J, Chen X, et al. Genetically encoded fluorescent sensors reveal dynamic regulation of NADPH metabolism. Nat Methods. 2017;14:720–8.
51. Fan J, Ye J, Kamphorst JJ, Shlomi T, Thompson CB, Rabinowitz JD. Quantitative flux analysis reveals folate-dependent NADPH production. Nature. 2014;510:298–302.
52. Pardieu B, Pasanisi J, Ling F, Dal Bello R, Penneroux J, Su A, et al. Cystine uptake Inhibition potentiates front-line therapies in acute myeloid leukemia. Leukemia. 2022;36:1585–95.
53. Döhner H, Wei AH, Löwenberg B. Towards precision medicine for AML. Nat Rev Clin Oncol. 2021;18:577–90.
54. Chu X, Zhong L, Dan W, Wang X, Zhang Z, Liu Z, et al. DNMT3A R882H mutation drives Daunorubicin resistance in acute myeloid leukemia via regulating NRF2/NQO1 pathway. Cell Commun Signal. 2022;20:168.
55. Shang Q, Pan C, Zhang X, Yang T, Hu T, Zheng L, et al. Nuclear factor Nrf2 promotes glycosidase OGG1 expression by activating the AKT pathway to enhance leukemia cell resistance to cytarabine. J Biol Chem. 2023;299:102798.
56. Cheng C, Yuan F, Chen XP, Zhang W, Zhao XL, Jiang ZP, et al. Inhibition of Nrf2-mediated glucose metabolism by brusatol synergistically sensitizes acute myeloid leukemia to Ara-C. Biomed Pharmacother. 2021;142:111652.
57. Juszczak M, Tokarz P, Woźniak K. Potential of NRF2 Inhibitors-Retinoic acid, K67, and ML-385-In overcoming doxorubicin resistance in promyelocytic leukemia cells. Int J Mol Sci. 2024;25:10257.
58. DiNardo CD, Pratz K, Pullarkat V, Jonas BA, Arellano M, Becker PS, et al. Venetoclax combined with decitabine or Azacitidine in treatment-naive, elderly patients with acute myeloid leukemia. Blood. 2019;133:7–17.
59. Pollyea DA, Stevens BM, Jones CL, Winters A, Pei S, Minhajuddin M, et al. Venetoclax with Azacitidine disrupts energy metabolism and targets leukemia stem cells in patients with acute myeloid leukemia. Nat Med. 2018;24:1859–66.
60. Yu X, Wang Y, Tan J, Li Y, Yang P, Liu X, et al. Inhibition of NRF2 enhances the acute myeloid leukemia cell death induced by venetoclax via the ferroptosis pathway. Cell Death Discov. 2024;10:35.

Publisher's note